Technical Note: Evaluation of the Copernicus Atmosphere Monitoring Service Cy48R1 upgrade of June 2023

Henk Eskes[1], Athanasios Tsikerdekis[1], Melanie Ades[2], Mihai Alexe[2], Anna Benedictow[3], Yasmine Bennouna[4], Lewis Blake[3], Idir Bouarar[5], Simon Chabrillat[6], Richard Engelen[2], Quentin Errera[6], Johannes Flemming[2], Sebastien Garrigues[2], Jan Griesfeller[3], Vincent Huijnen[1], Luka Ilić[7], Antje Inness[2], John Kapsomenakis[8], Zak Kipling[2], Bavo Langerock[6], Augustin Mortier[3], Mark Parrington[2], Isabelle Pison[9], Mikko R.A. Pitkänen[10], Samuel Remy[11], Andreas Richter[12], Anja Schoenhardt[12], Michael Schulz[3], Valerie Thouret[4], Thorsten Warneke[13], Christos Zerefos[8], and Vincent-Henri Peuch[2]

[1]Royal Netherlands Meteorological Institute, De Bilt, the Netherlands
[2]European Centre for Medium-Range Weather Forecasts, Reading, UK
[3]Norwegian Meteorological Institute, Oslo, Norway
[4]CNRS and Université Paul Sabatier, Laboratoire d'Aérologie, Toulouse, France
[5]Max Planck Institute for Meteorology, Hamburg, Germany
[6]Belgian Institute for Space Aeronomy, BIRA-IASB, Brussels, Belgium
[7]Barcelona Supercomputing Centre, Barcelona, Spain
[8]Academy of Athens, Athens, Greece
[9]Laboratoire des Sciences du Climat et de l'Environnement, Paris, France
[10]Finnish Meteorological Institute, Helsinki, Finland
[11]HYGEOS, Lille, France
[12]Institute of Environmental Physics, University of Bremen, Bremen, Germany
[13]University of Bremen Campus GmbH, Bremen, Germany

Correspondence: Henk Eskes (henk.eskes@knmi.nl)

Abstract. The Copernicus Atmosphere Monitoring Service (CAMS) is providing daily analyses and forecasts of the composition of the atmosphere, including the reactive gases such as O_3, CO, NO_2, $HCHO$, SO_2, aerosol species and greenhouse gases. The global CAMS analysis system (IFS-COMPO) is based on the ECMWF Integrated Forecast System (IFS) for numerical weather prediction (NWP), and assimilates a large number of composition satellite products on top of the meteorological observations ingested in IFS. The CAMS system receives regular upgrades, following the upgrades of IFS. The last upgrade, Cy48R1, operational since 27 June 2023, was very major with a large number of code changes, both for COMPO and for NWP. The main COMPO innovations include the introduction of full stratospheric chemistry, a major update of the emissions, of the aerosol model, including the representation of secondary organic aerosol, several updates of the dust life cycle and optics, inorganic chemistry in the troposphere, and the assimilation of VIIRS AOD and TROPOMI CO. The CAMS Cy48R1 upgrade was validated using a large number of independent measurement datasets, including surface in situ, surface remote sensing, routine aircraft and balloon and satellite observations. In this paper we present the validation results for Cy48R1 by comparing with the skill of the previous operational system (Cy47R3), with the independent observations as reference, for the period October 2022 to June 2023 during which daily forecasts from both cycles are available. Major improvements in

skill are found for the ozone profile in the lower-middle stratosphere and for stratospheric NO_2 due to the inclusion of full stratospheric chemistry. Stratospheric trace gases compare well with ACE-FTS observations between 10-200 hPa, with larger deviations between 1-10 hPa. The impact of the updated emissions is especially visible over East Asia and is beneficial for the trace gases O_3, NO_2, and SO_2. The CO column assimilation is now anchored by IASI instead of MOPITT which is beneficial for most of the CO comparisons, and the assimilation of TROPOMI CO data improves the model CO field in the troposphere. In general the aerosol optical depth has improved globally, but the dust evaluation shows more mixed results. The results of the 47 comparisons are summarised in a score card, which shows that 83% of the evaluation datasets show a neutral or improved performance of Cy48R1 compared to the previous operational CAMS system, while 17% indicate a (slight) degradation. This demonstrates the overall success of this upgrade.

1 Introduction

The Copernicus Atmosphere Monitoring Service (CAMS, http://atmosphere.copernicus.eu) is the service component of the European Earth Observation programme Copernicus focussing on atmospheric composition (Peuch et al., 2022). The CAMS system was developed during a sequence of European research projects (Hollingsworth et al., 2008) and became an operational service in 2015. The CAMS global near-real time (NRT) service provides daily analyses and 5-day forecasts of reactive trace gases and aerosol concentrations, and delayed-mode greenhouse gas analyses and forecasts. CAMS makes use of the measurements of the fleet of Copernicus Earth observation satellites, the Sentinels, as well as other relevant satellite and surface observations. Apart from the near-real time products CAMS produces global reanalyses for reactive gases and aerosols (Inness et al., 2019; Flemming et al., 2017) and greenhouse gases (Agustí-Panareda et al., 2023). CAMS is furthermore producing daily forecasts and analyses of air quality in Europe based on an ensemble of air quality models (Peuch et al., 2022; Marécal et al., 2015).

The global CAMS system is part of the Integrated Forecasting System (IFS) of ECMWF, the system used to produce the medium-range Numerical Weather Predictions (NWP) (ECMWF, 2024h). The modelling of reactive gases, aerosols and greenhouse gases is fully integrated in IFS (ECMWF, 2023). The assimilation of satellite data for atmospheric composition is part of the IFS 4D-Var data assimilation suite, and CAMS is assimilating the complete set of meteorological observations together with the composition data. CAMS forecasts are therefore combined weather-composition forecasts. The extended IFS system developed by CAMS for trace gases and aerosols is referred to as IFS-COMPO. A second CAMS system, IFS-GHG, is developed for CO_2 and CH_4 analyses, (high-resolution) forecasts, and reanalyses. This paper focuses on the evaluation of the IFS-COMPO NRT products.

The CAMS effort (Peuch et al., 2022) includes dedicated scientific activities to continuously develop and improve the modelling and satellite assimilation aspects of IFS-COMPO, including the chemistry code (Flemming et al., 2015; Huijnen et al., 2016, 2019), and the development of the aerosol scheme (Rémy et al., 2019, 2022). The data assimilation of reactive gases is described in Inness et al. (2015). Recent extensions relevant for Cy48R1 include the modelling of stratospheric chemistry (Huijnen et al., 2016; Chabrillat et al., 2023), the assimilation of TROPOspheric Monitoring Instrument (TROPOMI) CO

(Inness et al., 2022b) and Visible Infrared Imaging Radiometer Suite (VIIRS) AOD (Garrigues et al., 2023). Since Cy48R1 the IFS upgrade documentation also includes a chapter with a detailed discussion of the IFS-COMPO related modelling and data assimilation changes (ECMWF, 2023).

50   The CAMS service makes extensive use of independent measurement datasets of proven quality, available for different parts of the world, to evaluate the quality of the forecast/analysis and reanalysis products (Eskes et al., 2015; Katragkou et al., 2015; Lefever et al., 2015; Cuevas et al., 2015; Wagner et al., 2021; Agustí-Panareda et al., 2023). In total of the order of 65 measurement collections are used, obtained from observational networks like the Network for the Detection of Atmospheric Composition Change (NDACC), the World Meteorological Organisation Global Atmosphere Watch programme

55   (WMO-GAW), the Aerosol Robotic Network (AERONET), the In-service Aircraft for a Global Observing System (IAGOS), the Integrated Carbon Observation System (ICOS), the International Arctic Systems for Observing the Atmosphere (IASOA), and space organisations like the National Aeronautics and Space Administration (NASA), European Space Agency (ESA), the European Organisation for the Exploitation of Meteorological Satellites (EUMETSAT) and others. The CAMS global near-real time service component is evaluated in a series of validation reports produced every 3 months (Benedictow et al., 2023;

60   ECMWF, 2024d). The CAMS reanalysis validation reports for the aerosols and reactive gases (Bennouna et al., 2023) and greenhouse gases (GHG) (Ramonet et al., 2021) are updated on a yearly basis. Note that the production of the GHG reanalysis was interrupted (Agustí-Panareda et al., 2023) for a few years due to a degraded quality of the input satellite data. New system upgrades are evaluated before becoming operational, where CAMS Cy47R3 is discussed in Eskes et al. (2021), and Cy48R1 in Eskes et al. (2023b).

65   The ECMWF NWP and CAMS operational systems are upgraded at the same time and follow the same model cycles. A CAMS upgrade implies therefore a simultaneous upgrade of the NWP part of IFS in IFS-COMPO and IFS-GHG. The last upgrade, and topic of this paper, is the upgrade from Cy47R3 to Cy48R1, implemented on 27 June 2023. Upgrades normally occur at least once a year, but Cy48R1 is packing almost two years of developments. The delay is linked to the move of the ECMWF high-performance computing facilities from Reading, UK, to Bologna, Italy. As a result, Cy48R1 represents a very

70   major upgrade both for NWP and for CAMS. Detailed information about the ECMWF IFS upgrades can be found on ECMWF (2024h).

The CAMS pre-operational analyses and forecasts of CO_2 and CH_4 use an independent setup of the IFS. The upgrade of the greenhouse gas system to Cy48R1 took place on 27 February 2024, and a separate upgrade verification report was written (Langerock et al., 2024). The greenhouse gas products will not be discussed in this paper.

75   Before each upgrade, the new analysis and forecast configuration is operated as a so-called experimental suite or e-suite in parallel to the operational near-real time service (the o-suite, e.g., Cy47R3 in this paper) for about half a year. For the 27 June 2023 upgrade to Cy48R1, the e-suite run is available from 1 October 2022 to the moment of the upgrade, 27 June 2023. This implies that there are only a limited number of 9 months of data in the Autumn, Winter and Spring available to the evaluation, with a focus on wintertime. The choice to generate 9 months of e-suite data is made based on practical timing and computer

80   resources considerations. The length of the e-suite run has been discussed in the CAMS team, and for the next upgrade to Cy49R1, planned for the end of 2024, the e-suite will hopefully cover a full year. CAMS is also producing control runs without

the assimilation of atmospheric composition data. The control run allows us to distinguish changes due to the model from changes due to the assimilation of the atmospheric composition observations.

In this paper, the validation results are presented from comparisons of the performance of the Cy48R1 e-suite runs and e-suite control run with the operational run (o-suite and o-suite control run), all compared with independent observations. Prior to the upgrade, a preliminary evaluation of the new cycle was presented in a CAMS report (Eskes et al., 2023b), but this evaluation covered a relatively short period of about 5 months of CAMS results that were available at the time. This paper extends the validation by several months by including e-suite and o-suite analyses and forecasts up to the day of the upgrade, leading to more refined conclusions.

In section 2 we summarise the changes implemented in Cy48R1, and in section 3 we provide an overview of the validation datasets used. The validation results are shown in section 4 in the form of a series of plots comparing e-suite, o-suite and independent observations.

2   Overview of the CAMS global system

The operational CAMS global system provides analyses of the atmospheric composition of aerosols and reactive gases world-wide by blending satellite data and atmospheric simulation through a process called data assimilation. An overview of all satellite datasets assimilated in the CAMS global system can be found in Peuch et al. (2022) and Eskes et al. (2023b). Further details on the different production runs and their data usage can be found at the CAMS global products website (ECMWF, 2024e). The history of CAMS system upgrades, the data products, the satellite data assimilated (and monitored) and relevant references, is available in the CAMS data documentation website (ECMWF, 2024b), while the results of the operational satellite data monitoring is available at the CAMS data monitoring website (ECMWF, 2024c). CAMS is continuously extending its activity by testing and using new emerging datasets such as trace gas retrievals from the geostationary Geostationary Environmental Monitoring Spectrometer (GEMS) and Tropospheric Emissions: Monitoring of Pollution (TEMPO), improved retrievals from past and present missions, and preparing for future missions such as Sentinels 4 and 5.

Copernicus products are made available for free. The CAMS products can be accessed through the Atmosphere Data Store (ADS) at https://ads.atmosphere.copernicus.eu/. The available o-suite output includes: analysis fields available every 3 hours, for the two 12-hour analysis windows per day; twice daily 5-day forecast starting from the analysis at 00 and 12 UTC, with 2D fields available hourly, and 3D fields available every 3 hours. The output includes a large number of trace gases, aerosol composition and optical properties of the aerosols, as detailed on the ADS. Most of the comparisons documented below make use of the first 24 hours of the forecast runs starting 00 UTC, which allows a direct comparison with the control run. For some comparisons the analysis results were used, as indicated.

A control run is produced both for the e-suite (e-suite control run) and o-suite (o-suite control run). These runs are useful to distinguish the impact of data assimilation changes from the impact of modelling changes. The control run applies the same settings as the respective o-suite and e-suite, but the data assimilation is not switched on for atmospheric composition. The

meteorology in the control run is initialised with the meteorological fields from the o-suite (or e-suite). The control run archive contains 5-day forecasts starting from the 00 UTC analysis.

The global forecasting system is continually being evaluated to ensure the output meets the expected requirements. Comprehensive Evaluation and Quality Assurance (EQA) reports are provided for the CAMS system on a quarterly basis (ECMWF, 2024d). CAMS uses a multitude of independent data sets to routinely monitor its global forecasts. It works with various data providers, acquiring the observations with appropriate timelines and generating graphics that show the differences between the forecasts and the independent observations (ECMWF, 2024g). The two main websites are the global evaluation server for near-real time analysis and forecast products (ECMWF, 2024f) and the AeroVal evaluation server to evaluate the reanalysis products (ECMWF, 2024a).

In the next subsections the model, data assimilation and emissions upgrades of the CAMS e-suite (Cy48R1) are summarised, and the observations used are introduced.

2.1 The CAMS e-suite (Cy48R1)

This upgrade encompasses several significant scientific advancements. A detailed documentation of the CAMS Cy48R1 upgrade for aerosols and reactive gases is available at ECMWF (2023). More information regarding the aerosol/chemistry changes and the meteorological changes are provided in IFS (2024) and CAMS (2024) respectively. In the following subsections the model, assimilation and emissions updates are summarised.

2.1.1 Model updates

The CAMS IFS cycle Cy48R1 is based on the ECMWF's IFS cycle Cy48R1. The model consists of gas-phase chemistry modules for the troposphere (based on CB05 scheme, see Williams et al. (2022) and references therein) and the stratosphere (based on the Belgian Assimilation System for Chemical ObsErvations (BASCOE) scheme, see Errera et al. (2019), Huijnen et al. (2016) and references therein) that includes 123 active tracers. The distinction between the tropospheric and stratospheric chemistry schemes occurs at the tropopause, which is determined based on the temperature lapse rate of the model. The aerosol scheme AER (originally based on LOA/LMDZ model, Reddy (2005)) is a bulk-bin scheme that consists of 16 active species, which are coupled with the chemistry schemes in various ways (ECMWF, 2023).

Before Cy48R1 only ozone was modelled in the stratosphere using a linear parameterization. The stratospheric chemistry module activated in Cy48R1 (Huijnen et al., 2016) is a re-implementation of the Belgian Assimilation System for Chemical ObsErvations (BASCOE) chemical module and it involves 64 species engaging in 157 gas-phase, 9 heterogeneous, and 53 photolytic reactions (Errera et al., 2019). It encompasses ozone-depleting substances, greenhouse gases, and other species vital for comprehensive stratospheric ozone photochemistry (Chabrillat et al., 2023). Additionally, basic sulphur chemistry is included to represent gas-phase sulphuric acid formation and enable coupling with the sulphate aerosol module, featuring OCS, SO_2, SO_3, and H_2SO_4 reactions. Note that the 64 tracers listed as active in stratospheric chemistry include HCN and CH_3CN, as well as the tracers to represent sulphur chemistry, which are additions specific to CAMS, on top of the default BASCOE chemistry with 58 species described in Errera et al (2019).

In the troposphere, inorganic chemistry was updated, hydrogen cyanide (HCN) and acetonitrile (CH$_3$CN) are now included as long-lived tracers, serving as indicators of biomass burning activity. For the degradation of organic compounds, the basic isoprene oxidation scheme was replaced with a more explicit approach based on Stavrakou et al. (2010), further modified according to Lamarque et al. (2012) and Myriokefalitakis et al. (2020). This updated scheme contains reaction products including glyoxal (CHOCHO), glycolaldehyde, isoprene-peroxide, hydroxy-acetone, and two hydroxy-aldehydes (Williams et al., 2022). The scheme was further expanded to include an explicit parameterization of aromatics tracers xylene and toluene, acting as precursors for Secondary Organic Aerosol (SOA).

Recent developments of the CAMS aerosol modelling are described in Rémy et al. (2022). The Cy48R1 upgrade introduced notable changes in aerosol. The SOA species are now represented with dedicated tracers, distinguishing biogenic and anthropogenic origins, and coupled with the tropospheric chemistry for their production. The e-folding time that converts hydrophobic components of Organic Matter (OM) and Black Carbon (BC) into hydrophilic forms has been decreased to 2.8 hours from 1.16 days. The assumed number size distribution for dust, which used to compute the offline dust aerosol optical properties (mass extinction, single scattering albedo and asymmetry parameter), has been updated based on values from Ryder et al. (2018) derived from aircraft measurements over the tropical Eastern Atlantic. The refractive index has also been updated. The dust source function, that is used to modulate dust emissions, has been recomputed based on a three-year analysis of the MIDAS product (Gkikas et al., 2021), leading to monthly variations instead of fixed yearly values. A regional redistribution of total dust emissions into the three dust bins has been implemented, based on long simulations of dust mineralogy, which directs relatively more emissions to finer dust bins (1 and 2) compared to CY47R3. The dust mass emissions and burden are significantly higher in Cy48R1 (see details on ECMWF (2023)), which leads to an increase of dust optical depth globally by about 30%. Note however that the Mass Extinction Coefficient (MEC), which is calculated by dividing aerosol optical depth to aerosol mass is reduced for dust in Cy48R1 (Figure S1). Thus, although dust optical depth increases, dust mass extinction efficiency decreases. A new parameterization for the rebound effect of super-coarse dust particles over continental surfaces, relying on Zhang (2001) was added, which reduces dry deposition for those particles. In addition, sedimentation, previously limited to super-coarse dust and sea-salt, is now applied broadly to all aerosol tracers, although the impact is mainly significant in the stratosphere, where sedimentation is the dominant sink.

The aerosol optical properties of aerosols have received several updates in Cy48R1. The inclusion of a specific SOA species distinguishes primary from secondary OM. The new set of optical properties for OM, based on Brown et al. (2018), leads to higher extinction, particularly at low relative humidity conditions. Notably, the refractive index used in Cy48R1 results in more absorbing organic matter in the UV and near-UV regions, characterised as brown carbon. Further, a scaling factor (1.375) on mass extinction of sulphate aerosol, previously based on the molar mass ratio of ammonium sulphate to sulphate, has been removed as ammonium is now a separate species (since cycle 46R1).

Nitrate and Ammonium aerosols were added to the aerosol species in Cy46R1 whilst simultaneously the SO$_2$ precursor was removed. However, the update to the new species as part of the aerosol data assimilation process was not correctly included (see Benedetti et al. (2009) for a full description of the aerosol assimilation process). This was fixed in Cy48R1, leading to increments now being added to both fine and coarse nitrate and ammonium.

2.1.2 Assimilation updates

The assimilated products in the operational CAMS system is visualised in Figure S2. The assimilation of TROPOMI total column CO became operational at the 28th of April 2023 in Cy48R1 (only the last months of the e-suite period). The impact of this inclusion was tested from July to December 2021 (Inness et al., 2022a). The results showed an 8% increase in CAMS total column CO. The assimilation impact was significant during periods of high CO emissions from boreal wildfires in July and August 2021. While TROPOMI CO assimilation enhanced column constraints, it had limited influence on individual plumes transported across continents and oceans above 500 hPa.

The CAMS aerosol data assimilation system has depended on the Moderate Resolution Imaging Spectroradiometer (MODIS) instrument for more than ten years. To ensure forecast continuity, as the MODIS instrument is aging, the assimilation of AOD from NOAA VIIRS AOD from the Suomi National Polar-orbiting Partnership (S-NPP) and the NOAA-20 satellite was tested (Garrigues et al., 2023) and was activated in CY47R3 in February 2023 and is also active in CY48R1. Experiments assimilating VIIRS on top of MODIS or in place of MODIS in IFS cycle have been carried out from June to November 2020. A comparison with AERONET revealed that both experiments resulted in overall lower bias, notably in Europe, Africa, and Southeast Asia, with substantial improvements over desert and maritime aerosol sites.

The assimilation of data from different satellite instruments can introduce biases compared to each other or the model. To address this, a bias correction scheme, known as Variational Bias Correction (VarBC), is employed. VarBC introduces additional degrees of freedom, represented as bias parameters, into the 4D-Var cost function's observational term. Observational datasets that do not use VarBC are considered anchors and are crucial for preventing drifts in the fields (Inness et al., 2013). Note that in Cy48R1 the anchor for CO was changed from MOPITT (Terra) to IASI (Metop-C) and TROPOMI (Sentinel-5p), while the new anchor for AOD is now VIIRS (on the NOAA-20 satellite).

Cy48R1 includes a new volcanic SO_2 tracer (VSO2) in addition to the SO_2 tracer. VSO2 is currently not coupled to the chemistry yet but uses an e-folding lifetime of 7 days. TROPOMI SO_2 data with layer height information are assimilated into the VSO2 tracer following the method described in Inness et al. (2022a).

On 15 December 2022, still in Cy47r3, an update of the background error covariance wavelet file was implemented to use the correct NWP background errors. The update leads to considerably improved NWP forecast scores. As a consequence, changes to AOD and upper tropospheric and lower stratospheric ozone are also expected. The comparisons presented below cover the period October 2022 - June 2023. The impact of this change is observed in ozone when comparing the first two months with the months in 2023.

2.1.3 Emission updates

CAMS emissions are available from gridded inventories per sector (Denier van der Gon et al., 2023) except the emissions from dust and sea salt aerosols which are calculated online (ECMWF, 2023). Most emission inventories are on a monthly resolution capturing the seasonal cycle. Only the emissions for biomass burning coming from GFAS v1.4 (Kaiser et al., 2012) are provided in daily temporal resolution, including injection heights. Specifically in Cy48R1, the model uses anthropogenic emissions from

215　CAMS-GLOB-ANT v5.3 (Soulie et al., 2023), aviation emission from CAMS-GLOB-AIR v1.1, biogenic emissions from a climatology constructed from CAMS-GLOB-BIO v3.1 (Sindelarova et al., 2022) and natural emissions of DMS over the ocean from CAMS-GLOB-OCE v3.1. For reference, in Cycle 47r3 the anthropogenic emissions were based on CAMS-GLOB-ANT v4.2 and biogenic emissions from CAMS-GLOB-BIO v3.1.

Natural emissions use a monthly mean climatology. For varying volcanic SO_2 emissions, a climatology is constructed
220　based on recent satellite-based inventories (Carn et al., 2017). In Cy48r1 a sector-specific treatment for any of the emissions is introduced, allowing sector-specific diurnal cycle profiles and injection heights, see section 3.1.1 in ECMWF (2023) and Guevara et al. (2021) for more details.

3　Observations used for the validation of the CAMS system

The CAMS service includes activities dedicated to the validation of the global and regional (European) service products. The
225　latest validation results for the CAMS-global near-real time service (the o-suite) products can be found in Warneke et al. (2024), available at ECMWF (2024d), and the activity is described in Eskes et al. (2015). All CAMS validation reports for the global service products and the verification websites can be found at ECMWF (2024g).

The CAMS validation activity makes use of about 65 measurement datasets. It covers concentrations from the surface up to the stratosphere, using a wide range of instruments and measurement techniques, including surface in-situ, surface remote
230　sensing, aircraft and balloon in-situ, and satellite observations.

The observational datasets used for the evaluation of the Cy48R1 upgrade are summarised in Table 1. A description of all these diverse measurement datasets is beyond the scope of this paper. More details on the observation networks, instruments, measurement datasets and quality control can be found in the CAMS observations document Eskes et al. (2023a) and in the list of references included in this document.

235　The CAMS daily forecast and analysis products are evaluated on a regular 3-monthly basis. In practice this implies that only datasets can be used that are available within one month after real time. With several networks, such as NDACC, IAGOS or EEA surface observations, special arrangements (contracts) have been made such that near-real time unvalidated data can be used. For instance, the IAGOS NRT data are only available for operational users such as the weather and air quality services (e.g. CAMS). These data are inspected and validated by the instrument PI using a semi-automatic approach, and become
240　available as preliminary Level 1 (L1) data with a time-delay of a few days, as described in Nédélec et al. (2015) for ozone and CO, and in Petzold et al. (2015).

Many of the forecast-minus-observation results shown below make use of the following three metrics: the Modified Normalised Mean Bias (MNMB; a symmetric and normalised form to express the mean bias), the Fractional Gross Error (FGE; a symmetric and normalised absolute mean difference), and the Correlation (R). The scoring recommendations and metrics are
245　discussed in Tsikerdekis et al. (2023).

Table 1. Observational datasets used for the evaluation of the CAMS Cy48R1 e-suite.

Instrument	Species, property	Type, region	Network, provider	URL
Surface in-situ	O_3, CO, NO_2, SO_2, PM10, PM2.5	Europe	EEA-Airbase	https://eea.europa.eu
Surface in-situ	O_3, CO, NO_2, SO_2, PM10, PM2.5	China	CNEMC	http://www.cnemc.cn/en/
Surface in-situ	O_3, NO_2, PM10, PM2.5	USA	AirNow	https://www.airnow.gov
Surface in-situ	O_3, CO	Global	WMO-GAW	https://community.wmo.int/en/ activity-areas/gaw
Surface in-situ	O_3	Global	ESRL/GMD	https://www.esrl.noaa.gov
Surface in-situ	O_3	Arctic	IASOA	https://arctic.noaa.gov/research/ international-arctic-systems-for -observing-the-atmosphere/
Aircraft in-situ	O_3, CO	Airports	IAGOS	(http://www.iagos.org)
Ozonesonde	O_3	Global	NDACC	https://ndacc.larc.nasa.gov
Surface remote sensing	O_3, CO	Global	NDACC	https://ndacc.larc.nasa.gov
Surface remote sensing	AOD, AOD coarse, AE	Global	AERONET	https://aeronet.gsfc.nasa.gov/
IASI	O_3, CO	Satellite	EUMETSAT	https://www.esa.int/ Applications/Observing_ the_Earth/Meteorological_ missions/MetOp/About_IASI
MOPITT	CO	Satellite	NASA	https://terra.nasa.gov/
TROPOMI	NO_2, HCHO	Satellite	ESA	https://sentinels.copernicus. eu/web/sentinel/missions/ sentinel-5p
ACE-FTS	Stratospheric trace gases	Satellite	CSA	http://www.ace.uwaterloo.ca
MLS	Stratospheric trace gases	Satellite	NASA	https://mls.jpl.nasa.gov
SAGE-III	O_3	Satellite	NASA	https://sage.nasa.gov
OMPS-LP	O_3	Satellite	NASA	https://www.earthdata.nasa. gov/sensors/omps
UV stations	UV-Index	Global	Collected by FMI	https://fmi.fi

4 Results: changes in atmospheric composition introduced by Cy48R1

In this section we will summarise the main findings of the comparison of the e-suite (Cy48R1) and o-suite (Cy47R3), where both are evaluated with the independent observational data sets discussed above. This is presented for individual trace gases and aerosol properties, for the available observational data sets and for regions of interest. The evaluation is done for the period 01/10/2022 to 27/06/2023 where forecast results for both cycles are available. The corresponding e-suite control run (e-control)

250

and o-suite control run (o-control), without the assimilation of the atmospheric composition satellite data, were also evaluated. The improvement in performance of e-suite compared to the o-suite is summarised in Table 2 for all of the observational data sets used for the evaluation. The individual entries of this scorecard are discussed in the subsections below.

4.1 Ozone (O$_3$)

255 The ozone concentrations simulated by CAMS e-suite and o-suite were evaluated using several surface measurements provided by WMO-GAW, NOAA Earth System Research Laboratories (ESRL), IASOA, the European Environment Agency air quality database (EEA-Airbase), the China National Environmental Monitoring Centre (CNEMC) and the USA AirNow, profile measurements from IAGOS and ozonesondes, and satellite total column observations from the Infrared Atmospheric Sounding Interferometer (IASI).

260 The comparison against surface observations over Europe (EEA-Airbase), Fig. 1, shows that the MNMB of the e-suite is higher than the o-suite by up to 15% especially over Central and Northern Europe, changing some small underestimates in small overestimates. The e-suite temporal correlation improved slightly compared to the o-suite, but not everywhere. The bias in the e-suite control run is slightly lower and improved compared to the o-suite control run, in agreement with comparisons with WMO-GAW and ESRL/GMD observations.

265 The surface ozone validation using observations from the China National Environmental Monitoring Center, Fig. 2, shows that both the e-suite and e-suite control runs reduce the negative bias observed for the o-suite and o-suite control runs over the north-eastern region extending from Shanghai to Beijing. A slight improvement is also found over the megacity of Guangzhou in the south. This indicates less titration of ozone due to improved NO$_2$ in the e-suite/e-suite control run, see also section 4.3 below, which is likely linked to the anthropogenic emission update. The performance of the e-suite remained almost similar to 270 that of o-suite in central and western China. The correlation on average is about 0.75, similar for all experiments.

The evaluation of surface ozone using the AirNow ground-based stations over North America, Fig. 3, shows that the over-estimation is slightly higher in the e-suite than in the o-suite (MNMB from +13% to +22%) while the temporal correlation (R) and FGE improved, especially for the control run. The higher ozone bias may be related to a slight underestimation of NO$_2$ in the e-suite compared to the o-suite (Figure S3). The differences between the assimilation and control runs demonstrate the 275 impact of the assimilation.

Surface ozone from the e-suite and o-suite was also compared to WMO-GAW, ESRL/GMD and Arctic IASOA surface station observations (Figure S4). During October 2022 to February 2023 there was no significant change in the surface ozone bias between CAMS e-suite and o-suite, with relative biases of less than -40% for most of the stations. Exception is the SPO station over the Antarctica, where the e-suite shows a higher negative bias (-50%) than in o-suite (-40%).

280 The e-suite and o-suite have been evaluated with IAGOS aircraft measurements of tropospheric ozone. The time series of the daily profiles at the Frankfurt airport show that the e-suite and the o-suite have a similar performance in general (Fig. 4). However, in the free troposphere (between 850 hPa and 350 hPa, approximately between 1.5 to 8.5 km) the e-suite control run shows a reduced bias compared to the other runs from both the e-suite and the o-suite from the beginning of the evaluation period until April. For May-June, the e-suite control run develops a negative bias and the results of the other e-suite and

o-suite runs are similar. This is more clearly depicted in the time series of the monthly scores by vertical layers at Frankfurt, which shows a better performance (MNMB and FGE) in the e-suite control run in the free troposphere in January-April and the degradation for May and June. The two controls runs show a seasonal difference, which is compensated for by the assimilation. At most airports worldwide the bias in the lower troposphere (pressure > 850 hPa) is slightly larger for the e-suite than for the o-suite, and in particular over airports located in Western Africa and Eastern Asia (not shown). In the free troposphere, the bias is about the same between the e-suite than in the o-suite for most visited airports for the analysis or the 1-day forecast (Figure S5). For the control run we observe larger differences, and the o-control shows mainly positive biases, the e-control mainly negative biases compared to IAGOS, see also Fig. 4. These differences are reduced and results are improved by the data assimilation in the free troposphere.

In the upper troposphere (evaluations based on flight level data with a potential vorticity below 2) ozone is overestimated and the results from the e-suite and the o-suite are very similar for all runs (Figure S6) except for the o-suite control run which presents slightly larger biases than the other runs over the Northern Atlantic and North America.

Tropospheric ozone profiles have also been compared to ozonesonde observations, see Fig. 5. The northern hemisphere profile difference can be considered statistically robust (p-value for tropospheric columns is below 0.01) and little difference is seen between the o-suite and e-suite in the troposphere. The e-suite control run shows a large negative bias in the upper troposphere and lower stratosphere (below 100hPa), while almost no bias is found in the lower troposphere, in agreement with the IAGOS comparisons. For the other regions, the number of profiles is much lower, and the differences between the o-suite and e-suite are mixed: in the Tropics and Antarctica, the bias in the lower troposphere is smaller for the e-suite, while the opposite is found in the Arctic and southern hemisphere mid-latitudes. The spread in the differences is similar for both runs. Note that the ozonesonde results in the troposphere, including the change in bias around March-April, are consistent with the IAGOS plots shown above. Note that there is no significant change in the number of sondes around this time.

The global maps of monthly mean total column ozone for October 2022 is compared with satellite observations from IASI, see Fig. 6 top row. Overall, the performance is somewhat improved in the e-suite, with slightly better distributions of the ozone columns compared to the o-suite. A bias feature over the tropical Pacific ocean in October 2022 has disappeared in the e-suite. This feature may be attributed to the issue with the background covariances in Cy47R3, which was solved on 15 December. The positive bias at low latitudes in October is smaller in the e-suite than in the o-suite. For December 2022, the difference between the e-suite and the o-suite is less prominent. The positive bias above the Pacific ocean is improved in the e-suite and remains mostly below 5%. There is hardly a difference between e-suite and o-suite for June 2023.

4.2 Carbon Monoxide (CO)

The simulated carbon monoxide of CAMS e-suite and o-suite was evaluated using surface observations from the WMO-GAW, EEA-Airbase, CNEMC and AirNow networks, vertical profiles from IAGOS aircrafts and NDACC FTIR measurements, and satellite total column retrievals from MOPITT and IASI.

Over China, the comparison with surface CO observations indicates an overall reduction in CO concentrations in the e-suite, which leads to a reduced positive bias and better performance in the megacities over north-eastern China and particularly over

Shanghai, Hangzhou and Beijing (Fig. 7). The negative bias and the FGE increased in the e-suite in the rest of China, including central China. Overall correlation range between 0.3 to 0.8 for most stations with a mean of 0.53 for the e-suite. The e-suite shows similar correlations as the o-suite. In the densely populated north-eastern part of China correlations are exceeding 0.6 over most stations. The reduction in CO can be linked to the emission update in Cy48R1.

Compared to surface CO observations from five WMO-GAW stations (Hohenpeissenberg, Jungfraujoch, Sonnblick, Zugspitze, and Monte Cimone, located in Europe) there was no significant change in the bias between CAMS e-suite and o-suite runs, which does not exceed ±10% in general (Figure S7). The correlation for the e-suite has slightly improved compared to the o-suite over Europe and the Cape Verde station in the Tropics.

The comparison of the CO mixing ratios against EEA-Airbase observations over Europe shows that e-suite perform better than o-suite in terms of bias and correlation over most stations (Figure S8). In all cases note that e-control scored better than o-control as well, hence the detected improvements at the surface mainly originate from the model changes rather than assimilation changes.

The e-suite has been evaluated with IAGOS measurements of CO (Level 1 data) at different airports. The time series of the daily profiles (curtain plots) of the MNMB at the Frankfurt airport are presented in Fig. 8. The e-suite shows a smaller negative bias than the o-suite at all altitudes for the analysis and the 1-day forecast. This is also shown in the time series of the monthly scores by layers at Frankfurt, with an analysis and forecast improvement for the e-suite in both the Lower Troposphere (LT) and the Free Troposphere (FT) (Figure S9). However, CO is still underestimated by both the e-suite and the o-suite with a larger bias in the LT than in FT. According to the fractional gross error (FGE) monthly values, the e-suite improvement over the o-suite is about -0.05 for most of the months in the LT against about -0.02 in the FT, while for correlation results, no notable difference is found (Figure S9). The control runs from the e-suite and o-suite show a different seasonal pattern of the bias with a notable increase of the bias starting in early spring for both models. Like for the the assimilated runs, the bias from the control run is smaller for the e-suite than from the o-suite but only until March. This can also be seen in the monthly scores time series (Figure S9). For the remaining months the performance is similar for both control runs in the lower troposphere and slightly better for the o-suite control run in the free troposphere. For all other airports worldwide the bias (MNMB) in the low troposphere is very similar for the e-suite and the o-suite. However and like at Frankfurt, at most visited airports the absolute differences (FGE) are better in the free troposphere for assimilated runs of the e-suite compared with those of the o-suite (Figure S10). Regarding the control run results, the results are similar for both models. In the upper troposphere, at cruise altitude, CO is underestimated by both the e-suite and the o-suite runs. Like in the free troposphere there is a clear improvement of the bias in the upper troposphere over all regions in the e-suite compared to the o-suite and in particular for the analysis (Figure S11).

The results of the comparison with satellite CO column retrievals from the IASI and MOPITT instruments are shown in Fig. 9. Averaging kernels have been used in these comparisons. The IASI total column CO observations are well reproduced by the CAMS e-suite in terms of absolute amounts and spatial distribution. The e-suite relative bias for December 2022 with reference to IASI stays mostly within 20%, with wide areas below 5% and some negative bias above the Southern Africa biomass burning area (up to 20%), and a positive bias around 60°S, and a negative bias over Antarctica. The e-suite performs much better than

12

the e-control, which shows negative biases for the major part of the globe up to 20% regularly and peak amounts above South Africa exceeding 40%. The o-suite has mostly a negative bias compared to IASI, up to 20% regularly and up to 30% over the Pacific. Rows four and five show the e-suite relative biases for March 2023 and June 2023, that support the previous findings also for the other seasons. The MOPITT comparison looks very different, as overall biases are smaller for the o-suite than for the e-suite. The e-suite shows widespread positive biases up to 20% which is not present in the o-suite. Only the negative biases of the o-suite up to 20% above Northern Africa improved to remain mostly below 10% in the e-suite. Similar observations are made for the additional months from different seasons. These results for CO total columns demonstrate changes in the bias correction implemented in the e-suite, which is now using IASI-C and TROPOMI as reference. Note, that TROPOMI CO data were not assimilated in the e-suite until 28th of April, so the impact of TROPOMI has not been explicitly evaluated here.

In 2023 Canada was suffering from a very extreme fire season, which started already in May, with intense fires in June and continuing during the Summer. The e-suite is showing pronounced enhancements in CO in June, linked to the large GFAS fire emissions over Canada inserted in the model. As shown in the figure, the amount of CO produced is underestimated by up to 20% compared to IASI, and the largest relative error in the global map is located over Canada in June. However, the e-suite compares well with MOPITT over Canada, demonstrating the differences between these two satellite products. Negative CO biases over Canada compared to IASI (but positive compared to MOPITT) are also found in July and August, as shown in the JJA-2023 validation report available at ECMWF (2024d).

Over the Arctic Sea we observe a large region with negative biases in March compared to IASI. Note that IASI data has less sensitivity in spring as compared to summer above the Arctic due to lower thermal contrast, which may explain part of the differences. The MOPITT results seem to indicate a similar underestimate, so a negative bias in the analysis is likely.

Comparisons were also made against CO partial columns and profiles from the FTIR instruments, part of the surface remote sensing NDACC network (Fig. 10). The scores for 13 NDACC stations are presented in Table S1 and S2 in the supplement. For tropospheric CO columns, the bias for the e-suite is reduced compared to the o-suite for almost all sites. Although correlations are similar for the o-suite and e-suite, the ratio of the standard deviation in the tropospheric columns for the e-suite and the FTIR time series is higher compared to the o-suite. The bias at the tropical sites has switched sign and is now positive. For stratospheric CO columns the bias for the e-suite is reduced significantly for the southern hemispheric sites and is now of the order of the measurement uncertainty. The southern hemisphere correlations are also higher for the e-suite (in particular for the Antarctic site Arrival Heights). For the northern hemisphere, the e-suite and o-suite perform similarly. The o-suite has a degraded performance during this period in the southern hemisphere (Wollongong and Lauder stations, where the tropospheric columns show an increased negative bias compared to the months before October 2022 and the stratospheric columns show a strong (+20%) positive bias. A direct comparison between the o-suite and e-suite should therefore be interpreted with care. The figure shows that for the e-suite a reduced positive bias remains in the stratosphere for this period. This can be considered an improvement compared to the o-suite performance prior to October 2022 (negative bias $< -20\%$) and past October 2022 (positive bias $> +20\%$).

As of 22 May 2023, wildfires have been raging across Canada's Alberta province for three weeks. IAGOS aircraft profiles of CO over Montreal and Calgary picked up the pollution plumes from these events, and have been compared with the CAMS

results (Figure S12). For most profiles studied during this event, the e-suite is performing better than the o-suite with values
of the CO mixing ratios higher than those provided by the o-suite, although the forecast model remains to face difficulties to
capture the high concentrations in the plumes, while the altitude is simulated with success.

4.3   Nitrogen dioxide (NO$_2$)

The CAMS configurations were also compared with surface observations in China, Europe and North America.

Over China (Fig. 11), the e-suite and e-suite control run significantly reduce the Cy47R3 positive offset in surface NO$_2$ over
most regions in eastern China , which also led to a reduced bias in surface ozone as discussed in section 4.1. The correlation
of the e-suite/e-suite control run is similar (slightly reduced) compared to the o-suite/o-suite control run. The mean correlation
coefficient averaged over all stations is 0.52 for the e-suite and 0.54 for the o-suite.

The comparison with surface NO$_2$ observations in Europe obtained from EEA-Airbase shows that the e-suite performs better
than o-suite in terms of bias for a majority of the stations especially in Central and Northern Europe (Figure S13). Interestingly,
this coincides with the regions where a slightly higher bias was found for ozone in the e-suite indicating a chemical regime
changes in the model. In terms of correlations the e-suite and o-suite performed almost equally.

The evaluation of surface NO$_2$ using the AirNow ground-based stations over North America shows that the underestimation
in e-suite/e-suite control run is higher than o-suite/o-suite control run (from about -30% to -40%) while the temporal correlation
(R) slightly improves (from 0.49 to 0.54) (Figure S3).

The CAMS e-suite Cy48R1 tropospheric NO$_2$ column data is compared to the TROPOMI scientific IUP Bremen tropo-
spheric NO$_2$ product, see Figure 12. Three different months are selected for performance demonstration, including those
periods with highest and lowest solar elevation for the two hemispheres. Overall, the e-suite results correspond well with
the observational data in terms of spatial and temporal variations and absolute amounts. However, there are also apparent
differences between model and measurements. Largest differences are mainly observed above regions with major emissions.
Locations strongly affected by anthropogenic pollution such as hotspots in China can show strong positive biases partly above
100%. In comparison to the o-suite, however, the e-suite performs better compared to TROPOMI especially above strongly
polluted regions such as Eastern China. Here, the positive bias in the o-suite is reduced in the e-suite as well as above other
hotspot regions. This effect is best visible in the December maps (left column of Fig. 12). This improvement is likely due
to the updated emissions used in Cy48R1. Most areas with strong positive biases are smaller in spatial extent in the e-suite
compared to the o-suite, and smaller in their bias values. In addition, there are a few confined regions, where the e-suite shows
positive biases not present in the o-suite comparison such as above the North Sea. This can mainly be explained by the lower
anthropogenic emissions in CAMS-GLOB-ANT v5.3 as applied in the e-suite, compared to CAMS-GLOB-ANT v4.2 in the
o-suite.

Some typical biomass burning areas such as Southern Africa or South America show negative biases around 40% compared
to TROPOMI. Negative biases are seen also above parts of the US, the Northern Atlantic, Northern Pacific and parts of Asia.
In contrast, positive biases are found over boreal fires. No noteworthy degradation in performance is seen when moving from
the previous o-suite to the e-suite results. This is also true concerning the background regions, both e-suite and o-suite perform

well in representing background values close to zero. The negative biases for some oceanic background regions are slightly larger for the e-suite than for the o-suite. The negative biases above the oceans on the Northern Hemisphere show up in areas where the absolute tropospheric NO_2 column is small and close to background levels. Slight differences in absolute amounts hence cause comparably large relative bias values. Overall, the performance of the e-suite is slightly better than the o-suite.

4.4 Sulfur dioxide (SO_2)

The comparison against SO_2 surface observations from the China National Environmental Monitoring Center shows that e-suite/e-suite control run significantly reduces the positive bias observed for the o-suite/o-suite control run over most regions in eastern China as indicated by the difference in FGE between e-suite and o-suite (Fig. 13. However, a high overestimation (>50%) is still observed in the e-suite for many of the stations, indicating a remaining possible overestimation of SO_2 emissions in the updated CAMS_GLOB_ANT inventory. Note that the temporal correlation (R) is slightly reduced in the e-suite compare to the o-suite.

The comparison of the SO_2 mixing ratio against EEA-Airbase observations over Europe shows that the e-suite/e-suite control run performs better than the o-suite/o-suite control run in terms of bias for most stations (Figure S14). The correlations are almost equal.

4.5 Formaldehyde (HCHO)

The tropospheric formaldehyde (HCHO) column from the CAMS e-suite is compared to the TROPOMI scientific IUP Bremen tropospheric HCHO product (Eskes et al., 2023a). Monthly mean global maps and differences are shown in Fig. 14.

The e-suite overestimates the tropospheric HCHO columns over South America and Northern Australia by more than 60% in December and March, and there is also an overestimation over Indonesia. The allocation of the HCHO columns over Northern and Southern Africa in the two months is well reproduced by the model, but there are biases in certain time periods, such as the overestimation North of the equator and an underestimation in the South for June 2023.

In comparison to the o-suite, the overestimation above South America and Northern Australia is stronger in the e-suite visible in the relative biases of the e-suite and the o-suite in row four and five of Fig. 14. This could be the effect of the updated isoprene chemistry, which induced a higher HCHO production. Above Northern Africa, the HCHO values show a larger positive bias, while over Southern Africa the negative bias is slightly less pronounced in the e-suite. Overall, the performance is similar, but slightly degraded for the e-suite.

4.6 Stratospheric ozone (O_3)

Stratospheric ozone from CAMS e-suite Cy48R1 and o-suite have been compared against satellite limb profiles and ozoneson-des, considering the analyses, the 5th day forecasts and the o-suite control run, see Fig. 15. The full e-suite period is considered, from 1 October 2022 to 27 June 2023.

The main conclusions are:

– In the lower stratosphere, at pressures higher than 10 hPa, the e-suite agrees better with the observations than the o-suite, with lower biases, lower FGE, and higher correlations for the 9-month period evaluated.

– The e-suite agrees much better with observations than the o-suite in the tropics.

– The e-suite 5-day forecast agrees better with independent observations than the o-suite during ozone hole conditions.

– In the upper stratosphere (at pressure lower than 10 hPa), the e-suite displays a larger negative bias than the o-suite, while the correlations are improved in the e-suite in the upper stratosphere in the tropics.

– The control run of the e-suite shows a higher negative bias than the o-suite control run in the upper stratosphere above the 10 hPa level.

The difference between the o-suite and the e-suite are largely due to the the introduction of full stratospheric chemistry, which is demonstrated by comparing the control runs of the o-suite and the e-suite.

Stratospheric ozone has also been compared to lidar profile observations from the NDACC network for the full e-suite period of 9 months, see Fig. 16. Above 10hPa the e-suite mean profile deviates from the o-suite, showing a negative bias compared to the lidar observations, increasing with altitude. Between 50hPa and 10hPa the e-suite overestimates the ozone concentration. The negative bias feature observed around 20 hPa in the o-suite at Mauna Loa is no longer present in the e-suite. The dispersion (std) in the differences is slightly, but systematically, improved for the e-suite. In general, the conclusions for the lidar comparisons are very similar to the satellite comparisons.

4.7 Other trace gases in the stratosphere

Other species simulated in the stratosphere in the e-suite have been compared with satellite limb profiles considering 3 hourly first day forecast. The new CAMS cycle 48R1 introduces full stratospheric chemistry, and meaningful comparisons with the o-suite is not possible. But reasonable concentration of these species are important because of their impact on ozone. Species considered are: CCl_4, $CFC-11$, $CFC-12$, $HCFC-22$, ClO, $ClONO_2$, HCl, CH_4, H_2O, HNO_3, N_2O, N_2O_5, NO_2, NOx $(NO+NO_2)$, and O_3.

There is a relatively good agreement between the e-suite and observations for long-lived species (CCl_4, $CFC-11$, $CFC-12$, CH_4, $HCFC-22$ and N_2O) and HCl between 10 hPa and 200 hPa, see Figure 17. The chemical H_2O tracer in the CAMS e-suite shows a negative bias. Even though not perfect, CAMS e-suite NO_2 (and NOx) agree relatively well with observations, which was not the case in the previous o-suite cycles. Above the 10 hPa level the concentrations are overestimated compared to ACE-FTS, and there is room for improvement. For ClO, the agreement is good against MLS, less good with ACE-FTS, but this dataset is supposed to be less reliable than MLS for this species.

Stratospheric NO_2 columns have been compared with TROPOMI retrievals, see Fig. 18. The observational NO_2 stratospheric column is represented well by the e-suite in terms of absolute amounts, latitudinal variation and temporal changes. Over the largest part of the globe, column amounts agree to within $2x10^{15}$ molec/cm^2, deviating by less than 10%. The e-suite performs well in reproducing the general strong increase in stratospheric NO_2 at high latitudes in the summer hemisphere.

4.8 UV radiation

While no changes to the UV code were implemented in Cy48R1, the surface UV index (UVI) forecasts are affected by the changes in the optical depth of trace gases (of which most notably stratospheric ozone), aerosols, and thick clouds. The net effect of these factors on the hourly forecast performance of the new model cycle were estimated using ground based UVI measurements as the reference data at the 38 stations, located in Europe, Israel, Thailand, Australia, New Zealand, and the Antarctic.

Figure 19 illustrates the statistical improvement of Cy48R1 compared with Cy47R3 when evaluated against the ground based observations in terms of MNMB, FGE, and R. MNMB and FGE included all available hourly UVI forecasts, while R included only UV forecasts close to local noon in order to emphasise the importance of atmospheric composition (instead of solar zenith angle SZA), and to highlight the time of day when UV radiation is typically most intense and hazardous. Overall, the statistics (mean MNMB=5 %, mean FGE=0.30, and mean R=0.82) indicate that CAMS UV forecasts are of good quality in Cy48R1. The mean values of R and FGE indicate no significant changes in correlation and scatter between the old and the new model cycles, however the mean MNMB increases slightly from 2 % to 6 %. This finding is supported by comparing the zonal mean of daily maximum UVI between the two model cycles, which increased by +0 to +4 % with the largest increase +2 to +4 % occurring between 50°S and 60°N in Cy48R1 compared to Cy47R3.

4.9 Aerosol

The Cy48R1 introduces a redistribution of aerosol optical depth per species (Fig. 20 first column). Starting from Cy48R1, the secondary organic aerosol (SOA) optical depth is now provided separately, whereas prior to this update, the SOA optical depth was included as part of the organic matter (OM) optical depth. For this report, the OM optical depth in the e-suite includes the SOA, in order to ensure comparability with the OM optical depth in the o-suite. Compared to o-suite there is less AOD for the e-suite particularly due to reduction in sulphate optical depth (Fig. 20 second column). For the e-suite there is less black carbon optical depth, particularly over Central Africa. Over southeast Asia and Sahel nitrates optical depth decreases by about 50% in the e-suite compared to the o-suite. Contrarily, the sea salt and ammonium optical depth increases while dust and organic matter changes are regionally dependent. The Ångström Exponent (AE), a parameter which is indicative of the aerosol size distribution, is considerably lower globally (reduction by -0.12) in e-suite, especially over Middle East and Sahara, while it increased over South Africa, South America and Australia.

These changes are related to (1) the introduction of two new secondary organic aerosol tracers (anthropogenic and biogenic) along with their respective precursor gas tracers (2) modifications to dust emissions and removal simulation that increased the global dust mass burden by a factor of 2, (3) a review of aerosol optical properties for dust and brown carbon, as well as (4) improvements on secondary inorganic aerosol simulation. Note that the AOD and AE mostly increases due to assimilation, except for dust (Fig. 20 third column).

The evaluation of daily Aerosol Optical Depth (AOD) and Ångström Exponent (AE) against the ground based network of AERONET version 3 level 1.5 stations shows that e-suite overestimates less compared to o-suite for both parameters (Fig.

21 and Fig. 22). The e-suite improves in terms AOD MNMB globally (from +21% in o-suite to +7% in e-suite), especially over North America, Europe, East Asia and Middle East. Over South-East Asia and Sahara the MNMB performance remains almost unchanged. Notably for South Asia a deterioration in performance (higher underestimation) is observed compared to the o-suite. The correlation (R) performance remains unchanged (approximately 0.70 in both o-suite and e-suite). Note that both control runs are underestimating AOD (not shown).

The AE, improves in terms of global bias (Mean Bias from +0.28 in o-suite to +0.19 in e-suite), with regional improvements in Europe, North America as well as East China (Fig. 22). The e-suite updated dust emissions and deposition fluxes, resulting in a coarser aerosol size distribution (smaller AE) and dust mass burden over the deserts in the e-suite control run. Results specifically to dust changes are discussed in subsection 4.11. The correlation (R) of global AE improves (from 0.34 in o-suite to 0.44 in e-suite), remains unchanged in Europe and East Asia, with a small improvement in South Asia, Sahara and Middle East and a considerable improvement over South and North America, though R still remains below 0.5 in the latter case (AeroVal, 2024).

4.10   Particulate matter

Global daily near real time data of particulate matter, under 10 (PM10) and 2.5 (PM2.5) micrometres in diameter, from the surface observational networks AirNow (North America, U.S. Environmental Protection Agency (EPA)), EEA-NRT-rural (Europe, European Environmental Agency (EEA)), and CNEMC (China National Environmental Monitoring Centre) are used to evaluate e-suite and o-suite experiments for the period October 2022 to June 2023 (Figure 23). Note that all stations are considered for the AirNow and CNEMC networks, including urban stations, hence CAMS may not be able to fully capture the very high PM2.5 and PM10 measured with the observations at local urban scale due to the coarse spatial resolution of the model. We focus in this section on the evaluation results for PM2.5. The results for PM10 were found to be very similar to that of PM2.5. They are presented at the Aeroval website (AeroVal, 2024) and are discussed in Eskes et al. (2023b).

Over North America and Europe, e-suite improves PM2.5 in terms of MNMB (-3.2% and 8.9% respectively) compared to the o-suite, which exhibited a small overestimation of about +9.5% and +16.2%. Contrary over China the MNMB of e-suite (-19.9%) the e-suite exhibits a higher and negative bias when considering the performance over all available stations compared to o-suite (+3.8%). The spatial distribution of MNMB over China forms a clear dipole pattern. The eastern side, that encompass most of China's mega cities, mostly overestimates PM2.5, while in the western part, that contains less populated high altitude regions, underestimates PM2.5. The PM2.5 of e-suite outperforms o-suite in the eastern part of the country, with lower than 25% MNMB in most stations, while the opposite stand for the western part, where e-suite display more negative than -50% MNMB in most stations. The measured PM2.5 over China displays a peak in January, which is strongly underestimated by both e-suite and o-suite (Figure 20). The correlation for e-suite and o-suite remains unchanged in Europe (about 0.47), slightly improves over China (from 0.55 to 0.57) and better in North America (from 0.39 to 0.55). The reduction of sulphates (Figure 20), the reduction of the PM2.5 positive bias (Figure 23) and the reduced positive bias of SO_2 over China (Figure 13) are linked to the reduced SO_2 emissions in e-suite.

4.11 Aerosol coarse

AOD coarse (AODc) of e-suite and o-suite were evaluated against the AERONET Spectral De-convolution Algorithm (SDA) version 3 level 1.5 daily data (Fig. 24). Overall, the e-suite AODc performs better than o-suite in terms FGE globally (from 1.09 to 0.77) and for all regions (except Middle East and Pacific/Australia/New Zealand). The same stands for the MNMB and R (not shown). Since the AE is indicative of the aerosol size distribution, its Mean Absolute Bias (MAB) reveals similar results.

Over and around arid areas AODc is represented mainly by aerosol dust. The new dust emission increased Dust Optical Depth (DOD) over Middle East and increased/decreased the DOD over the northern/southern part of the Sahara (Fig. 20e). Over North Africa the increasing dust concentration in spring, which increases AODc and decreases AE, is represented slightly better by e-suite compared to o-suite. Contrary in Middle East e-suite displays too high AODc (too low AE) compare to the observations. The simulated AODc and AE of e-suite is particularly better than o-suite over AERONET stations that are located over the westward transport of Saharan dust in N. Atlantic (e.g. Cape Verde), as well as other regions that are affected less from dust (e.g. southern Europe) (AeroVal, 2024).

5 Conclusions

The upgrade of the ECMWF/CAMS global system to Cy48R1 of 27 June 2023 involved many system changes in the composition modelling, emissions and assimilation which are listed in Section 2.1. The Cy48R1 represent a major upgrade and is the result of two years of model and data assimilation development. The upgrade introduces, among many other changes, a comprehensive stratospheric chemistry scheme with the addition of 63 gas species, contains important emissions updates, implements changes to the modelling of dust aerosol resulting in a redistribution of aerosol particles towards larger sizes and adds an explicit representation of secondary organic aerosol, and revisited isoprene and aromatics chemistry. In Cy48R1 the assimilation of TROPOMI CO and VIIRS AOD is introduced.

The validation results for in total 47 comparisons (measurement datasets) were summarised in the scorecard Table 2, which compares the relative performance of the new Cy48R1 configuration to the previous Cy47R3 system operational until 27 June 2023. The judgements presented in this summary table are qualitative, based on expert judgement and the investigation of maps and scores. The presentation of one quantitative score and significance assessment performed on all datasets, is in practice not feasible or meaningful. Each entry in the table has its own story, which is detailed in the results sections above. The datasets used for the assessment are very heterogeneous. Some datasets are very sparse (e.g. IAGOS where an extended datarecord is only available over Frankfurt) or cover only a limited region (e.g. surface concentrations from air-quality networks), while other networks are dense, such as AeroNet. Satellite data is available globally, but retrieval products for separate instruments (or the same instrument) often show significant differences and biases and uncertainties are not easy to assess. There are strong regional and seasonal differences in the scores reflecting differences in sources, processes, or aspects like aerosol composition.

The main results for the trace gases may be summarised as follows:

- The performance for CO has generally improved against all observations. The comparison against MOPITT is the exception. Previously, the assimilation system was anchored to MOPITT, while since Cy48R1 this is IASI. Furthermore, TROPOMI CO observations are now assimilated in Cy48R1. This anchoring change explains why the comparison with MOPITT is worse in the e-suite compared to the o-suite. However, the independent observations show that these changes are improvements.

- NO_2 and SO_2 show improved validation results against multiple observations, both at the surface and in columns observed from space. This may be linked to the upgrade of the emissions which are more realistically describing the emission trends in recent years.

- CAMS surface ozone and tropospheric ozone shows similar performance in e-suite and o-suite. However, ozone improvements are observed in Eastern China and the USA at the surface, probably linked to the emission update and changes in the precursors like NO_2.

- Stratospheric ozone below the 10 hPa level and total column ozone have improved against observations, especially in the Tropics. This may be linked to the inclusion of a full stratospheric chemistry scheme in Cy48R1. The bug fix in the formulation of the background covariances in Cy47R3 in December 2022 had a positive impact, especially for ozone in the tropics.

- The comparison of a large number of trace species in the stratosphere against ACE-FTS and MLS show realistic concentration profiles. This provides confidence in the implementation of stratospheric chemistry in IFS-COMPO.

- The overestimation of HCHO in the Tropics is more pronounced in the e-suite compared to TROPOMI. This may be related to the updated isoprene chemistry.

- The UV evaluation shows only minor changes.

The results for the aerosols may be summarised as follows:

- The aerosol optical depth evaluation shows improvements for most regions.

- The Ångström exponent, which is a measure representative of the aerosol size distribution, shows some improvement on the global scale but over the Middle East the performance deteriorates showing a too large fraction of coarse particles.

- Particulate matter (PM10 and PM2.5) at the surface is reduced in e-suite, which leads to lower bias in the eastern part of China compared to the o-suite. The e-suite and o-suite exhibits similar performance over North America and Europe.

It is important to note that the e-suite data is available for a period of about 9 months, with more emphasis on the NH Winter season. Therefore some results may not be fully representative for the entire year 2023 or for other years. The assimilation of TROPOMI CO in the e-suite was switched on only at the end of April 2023, and its impact could not be fully evaluated.

In summary, 55% of the evaluation datasets show an improved performance of Cy48R1 compared to the previous operational CAMS system, of which two improvements are indicated as major, 28% of the comparisons are neutral, and 17% indicate a degradation for the Cy48R1 e-suite compared to the Cy47R3 o-suite. This clearly indicates the overall success of the recent upgrade of the CAMS global system to Cy48R1.

The evaluation of the CAMS products with independent observations is continuously developing. Apart from further establishing interfaces with the major observation networks, CAMS is actively acquiring and testing (surface) data from South America, Africa, and Asian countries other than China. The scorecard presented in this paper is providing a qualitative summary of the results. More quantitative scoreboards are being developed for the quarterly o-suite validation reports, see Tsikerdekis et al. (2023).

The next upgrade of CAMS to Cy49R1 is planned for quarter 4 of 2024.

22

References

AeroVal: IFS-ESUITE: Evaluation of CAMS forecast and reanalysis models, https://aeroval.met.no/pages/evaluation/?project=cams2-82& experiment=IFS-ESUITE-Cy48R1, 2024.

Agustí-Panareda, A., Barré, J., Massart, S., Inness, A., Aben, I., Ades, M., Baier, B. C., Balsamo, G., Borsdorff, T., Bousserez, N., Boussetta, S., Buchwitz, M., Cantarello, L., Crevoisier, C., Engelen, R., Eskes, H., Flemming, J., Garrigues, S., Hasekamp, O., Huijnen, V., Jones, L., Kipling, Z., Langerock, B., McNorton, J., Meilhac, N., Noël, S., Parrington, M., Peuch, V.-H., Ramonet, M., Razinger, M., Reuter, M., Ribas, R., Suttie, M., Sweeney, C., Tarniewicz, J., and Wu, L.: Technical note: The CAMS greenhouse gas reanalysis from 2003 to 2020, Atmospheric Chemistry and Physics, 23, 3829–3859, https://doi.org/10.5194/acp-23-3829-2023, 2023.

Benedetti, A., Morcrette, J.-J., Boucher, O., Dethof, A., Engelen, R., Fisher, M., Flentje, H., Huneeus, N., Jones, L., Kaiser, J., et al.: Aerosol analysis and forecast in the European centre for medium-range weather forecasts integrated forecast system: 2. Data assimilation, Journal of Geophysical Research: Atmospheres, 114, https://doi.org/10.1029/2008JD011235, 2009.

Benedictow, A., Arola, A., Bennouna, Y., Bouarar, I., Cuevas, E., Errera, Q., Eskes, H., Griesfeller, J., Basart, S., Kapsomenakis, J., Langerock, B., Mortier, A., Pison, I., Pitkänen, M., Ramonet, M., Richter, A., Schoenhardt, A., Schulz, M., Tarniewicz, J., Thouret, V., Tsikerdekis, A., Warneke, T., and Zerefos, C.: Validation report of the CAMS near-real-time global atmospheric composition service Period December – February 2023, https://doi.org/10.24380/I31D-5I54, 2023.

Bennouna, Y., Arola, A., Benedictow, A., Blake, L., Bouarar, I., Cuevas, E., Errera, Q., Eskes, H., Griesfeller, J., Ilic, L., Kapsomenakis, J., Langerock, B., Mortier, A., I., P., Pitkänen, M., Richter, A., Schoenhardt, A., Schulz, M., Thouret, V., Tsikerdekis, A., Warneke, T., and Zerefos, C.: Validation report of the CAMS global reanalysis of aerosols and reactive trace gases, period 2003-2022, https://doi.org/10.24380/1rx8-mwi7, 2023.

Brown, H., Liu, X., Feng, Y., Jiang, Y., Wu, M., Lu, Z., Wu, C., Murphy, S., and Pokhrel, R.: Radiative effect and climate impacts of brown carbon with the Community Atmosphere Model (CAM5), Atmospheric Chemistry and Physics, 18, 17 745–17 768, https://doi.org/10.5194/acp-18-17745-2018, 2018.

CAMS, E. C.: Implementation of IFS cycle 48r1 for CAMS, https://confluence.ecmwf.int/display/FCST/Implementation+of+IFS+cycle+48R1, 2024.

Carn, S. A., Fioletov, V. E., McLinden, C. A., Li, C., and Krotkov, N. A.: A decade of global volcanic SO2 emissions measured from space, Scientific Reports, 7, https://doi.org/10.1038/srep44095, 2017.

Chabrillat, S., Minganti, D., Huijnen, V., and Remy, S.: Report documenting the changes in PSC parameterization and improvements of ozone hole forecasts, https://doi.org/10.24380/2NXV-H84F, 2023.

Cuevas, E., Camino, C., Benedetti, A., Basart, S., Terradellas, E., Baldasano, J. M., Morcrette, J. J., Marticorena, B., Goloub, P., Mortier, A., Berjón, A., Hernández, Y., Gil-Ojeda, M., and Schulz, M.: The MACC-II 2007–2008 reanalysis: atmospheric dust evaluation and characterization over northern Africa and the Middle East, Atmospheric Chemistry and Physics, 15, 3991–4024, https://doi.org/10.5194/acp-15-3991-2015, 2015.

Denier van der Gon, H., Gauss, M., Granier, C., Arellano, S., Benedictow, A., Darras, S., Dellaert, S., Guevara, M., Jalkanen, J.-P., Krueger, K., Kuenen, J., Liaskoni, M., Liousse, C., Markova, J., Prieto Perez, A., Quack, B., Simpson, D., Sindelarova, K., and Soulie, A.: Documentation of CAMS emission inventory products, https://doi.org/10.24380/Q2SI-TI6I, 2023.

ECMWF: IFS Documentation CY48R1 - Part VIII: Atmospheric Composition, https://doi.org/10.21957/749DC09059, 2023.

ECMWF: CAMS AeroVal evaluation server, https://cams2-82.aeroval.met.no, 2024a.

ECMWF: CAMS: Global atmospheric composition forecast data documentation, https://confluence.ecmwf.int/display/CKB/CAMS%3A+Global+atmospheric+composition+forecast+data+documentation, 2024b.

730 ECMWF: CAMS data monitoring, https://atmosphere.copernicus.eu/charts/packages/cams_monitoring/, 2024c.

ECMWF: CAMS Evaluation and Quality Assurance (EQA) reports, https://atmosphere.copernicus.eu/eqa-reports-global-services, 2024d.

ECMWF: CAMS global products, http://atmosphere.copernicus.eu/documentation-global-systems, 2024e.

ECMWF: CAMS global validation server, https://global-evaluation.atmosphere.copernicus.eu, 2024f.

ECMWF: CAMS global validation services, https://atmosphere.copernicus.eu/global-services, 2024g.

735 ECMWF: Changes to the forecasting system, https://confluence.ecmwf.int/display/FCST/Changes+to+the+forecasting+system, 2024h.

Errera, Q., Chabrillat, S., Christophe, Y., Debosscher, J., Hubert, D., Lahoz, W., Santee, M. L., Shiotani, M., Skachko, S., von Clarmann, T., and Walker, K.: Technical note: Reanalysis of Aura MLS chemical observations, Atmospheric Chemistry and Physics, 19, 13647–13679, https://doi.org/10.5194/acp-19-13647-2019, 2019.

Eskes, H., Huijnen, V., Arola, A., Benedictow, A., Blechschmidt, A.-M., Botek, E., Boucher, O., Bouarar, I., Chabrillat, S., Cuevas, E., et al.: Validation of reactive gases and aerosols in the MACC global analysis and forecast system, Geoscientific Model Development, 8, 3523–3543, https://doi.org/10.5194/gmd-8-3523-2015, 2015.

Eskes, H., Basart, S., Benedictow, A., Bennouna, Y., Blechschmidt, A.-M., Errera, Q., Hansen, K., Kapsomenakis, J., Langerock, B., Richter, A., Sudarchikova, N., Schulz, M., and Zerefos, C.: Upgrade verification note for the CAMS real-time global atmospheric composition service: Evaluation of the e-suite for the CAMS 47R3 upgrade of 12 October 2021, https://doi.org/10.24380/HFVP-FQ98, 2021.

745 Eskes, H., Basart, S., Benedictow, A., Bennouna, Y., Cuevas, E., Errera, Q., Kapsomenakis, J., Langerock, B., Pitkänen, M., Ramonet, M., Richter, A., Schönhardt, A., Schulz, M., Warneke, T., and Zerefos, C.: Observation characterisation and validation methods document, https://doi.org/10.24380/P5DE-SSQC, 2023a.

Eskes, H., Tsikerdekis, A., Benedictow, A., Bennouna, Y., Blake, L., Bouarar, I., Errera, Q., Griesfeller, J., Ilic, L., Kapsomenakis, J., Langerock, B., Mortier, A., Pison, I., Pitkänen, M., Richter, A., Schönhardt, A., Schulz, M., Thouret, V., Warneke, T., and Zerefos, C.: Upgrade verification note for the CAMS near-real time global atmospheric composition service: Evaluation of the e-suite for the CAMS CY48R1 upgrade of 27 June 2023, https://doi.org/10.24380/rzg1-8f3l, 2023b.

Flemming, J., Huijnen, V., Arteta, J., Bechtold, P., Beljaars, A., Blechschmidt, A.-M., Diamantakis, M., Engelen, R., Gaudel, A., Inness, A., et al.: Tropospheric chemistry in the Integrated Forecasting System of ECMWF, Geoscientific model development, 8, 975–1003, https://doi.org/10.5194/gmd-8-975-2015, 2015.

755 Flemming, J., Benedetti, A., Inness, A., Engelen, R. J., Jones, L., Huijnen, V., Remy, S., Parrington, M., Suttie, M., Bozzo, A., et al.: The CAMS interim reanalysis of carbon monoxide, ozone and aerosol for 2003–2015, Atmospheric Chemistry and Physics, 17, 1945–1983, https://doi.org/10.5194/acp-17-1945-2017, 2017.

Garrigues, S., Ades, M., Remy, S., Flemming, J., Kipling, Z., Laszlo, I., Parrington, M., Inness, A., Ribas, R., Jones, L., Engelen, R., and Peuch, V.-H.: Impact of assimilating NOAA VIIRS aerosol optical depth (AOD) observations on global AOD analysis from the Copernicus Atmosphere Monitoring Service (CAMS), Atmospheric Chemistry and Physics, 23, 10473–10487, https://doi.org/10.5194/acp-23-10473-2023, 2023.

Gkikas, A., Proestakis, E., Amiridis, V., Kazadzis, S., Tomaso, E. D., Tsekeri, A., Marinou, E., Hatzianastassiou, N., and García-Pando, C. P.: ModIs Dust AeroSol (MIDAS): a global fine-resolution dust optical depth data set, Atmospheric Measurement Techniques, 14, 309–334, https://doi.org/10.5194/amt-14-309-2021, 2021.

765 Guevara, M., Jorba, O., Tena, C., Denier van der Gon, H., Kuenen, J., Elguindi, N., Darras, S., Granier, C., and Pérez García-Pando, C.: Copernicus Atmosphere Monitoring Service TEMPOral profiles (CAMS-TEMPO): global and European emission temporal profile maps for atmospheric chemistry modelling, Earth System Science Data, 13, 367–404, https://doi.org/10.5194/essd-13-367-2021, 2021.

Hollingsworth, A., Engelen, R. J., Textor, C., Benedetti, A., Boucher, O., Chevallier, F., Dethof, A., Elbern, H., Eskes, H., Flemming, J., Granier, C., Kaiser, J. W., Morcrette, J.-J., Rayner, P., Peuch, V.-H., Rouil, L., Schultz, M. G., and Simmons, A. J.: TOWARD A
770 MONITORING AND FORECASTING SYSTEM FOR ATMOSPHERIC COMPOSITION: The GEMS Project, Bulletin of the American Meteorological Society, 89, 1147 – 1164, https://doi.org/https://doi.org/10.1175/2008BAMS2355.1, 2008.

Huijnen, V., Flemming, J., Chabrillat, S., Errera, Q., Christophe, Y., Blechschmidt, A.-M., Richter, A., and Eskes, H.: C-IFS-CB05-BASCOE: stratospheric chemistry in the Integrated Forecasting System of ECMWF, Geoscientific Model Development, 9, 3071–3091, https://doi.org/10.5194/gmd-9-3071-2016, 2016.

775 Huijnen, V., Pozzer, A., Arteta, J., Brasseur, G., Bouarar, I., Chabrillat, S., Christophe, Y., Doumbia, T., Flemming, J., Guth, J., Josse, B., Karydis, V. A., Marécal, V., and Pelletier, S.: Quantifying uncertainties due to chemistry modelling – evaluation of tropospheric composition simulations in the CAMS model (cycle 43R1), Geoscientific Model Development, 12, 1725–1752, https://doi.org/10.5194/gmd-12-1725-2019, 2019.

IFS, E. C.: Implementation of IFS Cycle 48r1, https://confluence.ecmwf.int/display/COPSRV/Implementation+of+IFS+cycle+48r1+for+
780 CAMS, 2024.

Inness, A., Baier, F., Benedetti, A., Bouarar, I., Chabrillat, S., Clark, H., Clerbaux, C., Coheur, P., Engelen, R. J., Errera, Q., Flemming, J., George, M., Granier, C., Hadji-Lazaro, J., Huijnen, V., Hurtmans, D., Jones, L., Kaiser, J. W., Kapsomenakis, J., Lefever, K., Leitão, J., Razinger, M., Richter, A., Schultz, M. G., Simmons, A. J., Suttie, M., Stein, O., Thépaut, J.-N., Thouret, V., Vrekoussis, M., Zerefos, C., and the MACC team: The MACC reanalysis: an 8 yr data set of atmospheric composition, Atmospheric Chemistry and Physics, 13,
785 4073–4109, https://doi.org/10.5194/acp-13-4073-2013, 2013.

Inness, A., Blechschmidt, A.-M., Bouarar, I., Chabrillat, S., Crepulja, M., Engelen, R., Eskes, H., Flemming, J., Gaudel, A., Hendrick, F., et al.: Data assimilation of satellite-retrieved ozone, carbon monoxide and nitrogen dioxide with ECMWF's Composition-IFS, Atmospheric chemistry and physics, 15, 5275–5303, https://doi.org/10.5194/acp-15-5275-2015, 2015.

Inness, A., Ades, M., Agustí-Panareda, A., Barré, J., Benedictow, A., Blechschmidt, A.-M., Dominguez, J. J., Engelen, R., Eskes, H., Flem-
790 ming, J., Huijnen, V., Jones, L., Kipling, Z., Massart, S., Parrington, M., Peuch, V.-H., Razinger, M., Remy, S., Schulz, M., and Suttie, M.: The CAMS reanalysis of atmospheric composition, Atmospheric Chemistry and Physics, 19, 3515–3556, https://doi.org/10.5194/acp-19-3515-2019, 2019.

Inness, A., Aben, I., Ades, M., Borsdorff, T., Flemming, J., Jones, L., Landgraf, J., Langerock, B., Nedelec, P., Parrington, M., and Ribas, R.: Assimilation of S5P/TROPOMI carbon monoxide data with the global CAMS near-real-time system, Atmospheric Chemistry and
795 Physics, 22, 14 355–14 376, https://doi.org/10.5194/acp-22-14355-2022, 2022a.

Inness, A., Ades, M., Balis, D., Efremenko, D., Flemming, J., Hedelt, P., Koukouli, M.-E., Loyola, D., and Ribas, R.: Evaluating the assimilation of S5P/TROPOMI near real-time SO_2 columns and layer height data into the CAMS integrated forecasting system (CY47R1), based on a case study of the 2019 Raikoke eruption, Geoscientific Model Development, 15, 971–994, https://doi.org/10.5194/gmd-15-971-2022, 2022b.

800 Kaiser, J. W., Heil, A., Andreae, M. O., Benedetti, A., Chubarova, N., Jones, L., Morcrette, J.-J., Razinger, M., Schultz, M. G., Suttie, M., and van der Werf, G. R.: Biomass burning emissions estimated with a global fire assimilation system based on observed fire radiative power, Biogeosciences, 9, 527–554, https://doi.org/10.5194/bg-9-527-2012, 2012.

Katragkou, E., Zanis, P., Tsikerdekis, A., Kapsomenakis, J., Melas, D., Eskes, H., Flemming, J., Huijnen, V., Inness, A., Schultz, M. G., Stein, O., and Zerefos, C. S.: Evaluation of near-surface ozone over Europe from the MACC reanalysis, Geoscientific Model Development, 8, 2299–2314, https://doi.org/10.5194/gmd-8-2299-2015, 2015.

Lamarque, J.-F., Emmons, L. K., Hess, P. G., Kinnison, D. E., Tilmes, S., Vitt, F., Heald, C. L., Holland, E. A., Lauritzen, P. H., Neu, J., Orlando, J. J., Rasch, P. J., and Tyndall, G. K.: CAM-chem: description and evaluation of interactive atmospheric chemistry in the Community Earth System Model, Geoscientific Model Development, 5, 369–411, https://doi.org/10.5194/gmd-5-369-2012, 2012.

Langerock, B., Kouyate, M., Ramonet, M., Warneke, T., and Eskes, H.: Upgrade verification note for the CAMS near-real-time global atmospheric composition service: Evaluation of the e-suite for the CAMS CY48R1 upgrade for the Greenhouse Gases CO2 and CH4, https://doi.org/10.24380/A3MD-6M2N, 2024.

Lefever, K., Van Der A, R., Baier, F., Christophe, Y., Errera, Q., Eskes, H., Flemming, J., Inness, A., Jones, L., Lambert, J.-C., et al.: Copernicus stratospheric ozone service, 2009–2012: validation, system intercomparison and roles of input data sets, Atmospheric chemistry and physics, 15, 2269–2293, https://doi.org/10.5194/acp-15-2269-2015, 2015.

Marécal, V., Peuch, V.-H., Andersson, C., Andersson, S., Arteta, J., Beekmann, M., Benedictow, A., Bergström, R., Bessagnet, B., Cansado, A., Chéroux, F., Colette, A., Coman, A., Curier, R. L., Denier van der Gon, H. A. C., Drouin, A., Elbern, H., Emili, E., Engelen, R. J., Eskes, H. J., Foret, G., Friese, E., Gauss, M., Giannaros, C., Guth, J., Joly, M., Jaumouillé, E., Josse, B., Kadygrov, N., Kaiser, J. W., Krajsek, K., Kuenen, J., Kumar, U., Liora, N., Lopez, E., Malherbe, L., Martinez, I., Melas, D., Meleux, F., Menut, L., Moinat, P., Morales, T., Parmentier, J., Piacentini, A., Plu, M., Poupkou, A., Queguiner, S., Robertson, L., Rouïl, L., Schaap, M., Segers, A., Sofiev, M., Tarasson, L., Thomas, M., Timmermans, R., Valdebenito, A., van Velthoven, P., van Versendaal, R., Vira, J., and Ung, A.: A regional air quality forecasting system over Europe: the MACC-II daily ensemble production, Geoscientific Model Development, 8, 2777–2813, https://doi.org/10.5194/gmd-8-2777-2015, 2015.

Myriokefalitakis, S., Daskalakis, N., Gkouvousis, A., Hilboll, A., van Noije, T., Williams, J. E., Sager, P. L., Huijnen, V., Houweling, S., Bergman, T., Nüß, J. R., Vrekoussis, M., Kanakidou, M., and Krol, M. C.: Description and evaluation of a detailed gas-phase chemistry scheme in the TM5-MP global chemistry transport model (r112), Geoscientific Model Development, 13, 5507–5548, https://doi.org/10.5194/gmd-13-5507-2020, 2020.

Nédélec, P., Blot, R., Boulanger, D., Athier, G., Cousin, J.-M., Gautron, B., Petzold, A., Volz-Thomas, A., and Thouret, V.: Instrumentation on commercial aircraft for monitoring the atmospheric composition on a global scale: the IAGOS system, technical overview of ozone and carbon monoxide measurements, Tellus B: Chemical and Physical Meteorology, https://doi.org/10.3402/tellusb.v67.27791, 2015.

Petzold, A., Thouret, V., Gerbig, C., Zahn, A., Brenninkmeijer, C. A. M., Gallagher, M., Hermann, M., Pontaud, M., Ziereis, H., Boulanger, D., Marshall, J., Nédélec, P., Smit, H. G. J., Friess, U., Flaud, J.-M., Wahner, A., Cammas, J.-P., Volz-Thomas, A., and Team, I.: Global-scale atmosphere monitoring by in-service aircraft – current achievements and future prospects of the European Research Infrastructure IAGOS, Tellus B: Chemical and Physical Meteorology, https://doi.org/10.3402/tellusb.v67.28452, 2015.

Peuch, V.-H., Engelen, R., Rixen, M., Dee, D., Flemming, J., Suttie, M., Ades, M., Agustí-Panareda, A., Ananasso, C., Andersson, E., Armstrong, D., Barré, J., Bousserez, N., Dominguez, J. J., Garrigues, S., Inness, A., Jones, L., Kipling, Z., Letertre-Danczak, J., Parrington, M., Razinger, M., Ribas, R., Vermoote, S., Yang, X., Simmons, A., de Marcilla, J. G., and Thépaut, J.-N.: The Copernicus Atmosphere Monitoring Service: from research to operations, Bulletin of the American Meteorological Society, https://doi.org/10.1175/bams-d-21-0314.1, 2022.

Ramonet, M., Langerock, B., Warneke, T., and Eskes, H.: Validation report of the CAMS greenhouse gas global reanalysis, years 2003-2020, https://doi.org/10.24380/438C-4597, 2021.

Reddy, M. S.: Estimates of global multicomponent aerosol optical depth and direct radiative perturbation in the Laboratoire de Météorologie Dynamique general circulation model, Journal of Geophysical Research, 110, https://doi.org/10.1029/2004jd004757, 2005.

Rémy, S., Kipling, Z., Flemming, J., Boucher, O., Nabat, P., Michou, M., Bozzo, A., Ades, M., Huijnen, V., Benedetti, A., et al.: Description and evaluation of the tropospheric aerosol scheme in the European Centre for Medium-Range Weather Forecasts (ECMWF) Integrated Forecasting System (IFS-AER, cycle 45R1), Geoscientific Model Development, 12, 4627–4659, https://doi.org/10.5194/gmd-12-4627-2019, 2019.

Rémy, S., Kipling, Z., Huijnen, V., Flemming, J., Nabat, P., Michou, M., Ades, M., Engelen, R., and Peuch, V.-H.: Description and evaluation of the tropospheric aerosol scheme in the Integrated Forecasting System (IFS-AER, cycle 47R1) of ECMWF, Geoscientific Model Development, 15, 4881–4912, https://doi.org/10.5194/gmd-15-4881-2022, 2022.

Ryder, C. L., Marenco, F., Brooke, J. K., Estelles, V., Cotton, R., Formenti, P., McQuaid, J. B., Price, H. C., Liu, D., Ausset, P., Rosenberg, P. D., Taylor, J. W., Choularton, T., Bower, K., Coe, H., Gallagher, M., Crosier, J., Lloyd, G., Highwood, E. J., and Murray, B. J.: Coarse-mode mineral dust size distributions, composition and optical properties from AER-D aircraft measurements over the tropical eastern Atlantic, Atmospheric Chemistry and Physics, 18, 17 225–17 257, https://doi.org/10.5194/acp-18-17225-2018, 2018.

Sindelarova, K., Markova, J., Simpson, D., Huszar, P., Karlicky, J., Darras, S., and Granier, C.: High-resolution biogenic global emission inventory for the time period 2000–2019 for air quality modelling, Earth System Science Data, 14, 251–270, https://doi.org/10.5194/essd-14-251-2022, 2022.

Soulie, A., Granier, C., Darras, S., Zilbermann, N., Doumbia, T., Guevara, M., Jalkanen, J.-P., Keita, S., Liousse, C., Crippa, M., Guizzardi, D., Hoesly, R., and Smith, S.: Global Anthropogenic Emissions (CAMS-GLOB-ANT) for the Copernicus Atmosphere Monitoring Service Simulations of Air Quality Forecasts and Reanalyses, Earth System Science Data Discussions, 2023, 1–45, https://doi.org/10.5194/essd-2023-306, 2023.

Stavrakou, T., Peeters, J., and Müller, J.-F.: Improved global modelling of HOx recycling in isoprene oxidation: evaluation against the GABRIEL and INTEX-A aircraft campaign measurements, Atmospheric Chemistry and Physics, 10, 9863–9878, https://doi.org/10.5194/acp-10-9863-2010, 2010.

Tsikerdekis, A., Eskes, H., and Schulz, M.: Scoring approaches for the evaluation of the CAMS global atmospheric composition forecasting system, https://doi.org/10.24380/3UFO-IC5K, 2023.

Wagner, A., Bennouna, Y., Blechschmidt, A.-M., Brasseur, G., Chabrillat, S., Christophe, Y., Errera, Q., Eskes, H., Flemming, J., Hansen, K. M., Inness, A., Kapsomenakis, J., Langerock, B., Richter, A., Sudarchikova, N., Thouret, V., and Zerefos, C.: Comprehensive evaluation of the Copernicus Atmosphere Monitoring Service (CAMS) reanalysis against independent observations, Elementa: Science of the Anthropocene, 9, https://doi.org/10.1525/elementa.2020.00171, 2021.

Warneke, T., Arola, A., Benedictow, A., Bennouna, Y., Blake, L., Bouarar, I., Errera, Q., Eskes, H., Griesfeller, J., Ilić, L., Kapsomenakis, J., Kouyate, M., Langerock, B., Mortier, A., Pison, I., Pitkänen, M., Ramonet, M., Richter, A., Schoenhardt, A., Schulz, M., Tarniewicz, J., Thouret, V., Tsikerdekis, A., and Zerefos, C.: Validation report of the CAMS near-real-time global atmospheric composition service: September – November 2023, https://doi.org/10.24380/90z9-nva, 2024.

Williams, J. E., Huijnen, V., Bouarar, I., Meziane, M., Schreurs, T., Pelletier, S., Marécal, V., Josse, B., and Flemming, J.: Regional evaluation of the performance of the global CAMS chemical modeling system over the United States (IFS cycle 47r1), Geoscientific Model Development, 15, 4657–4687, https://doi.org/10.5194/gmd-15-4657-2022, 2022.

Zhang, L.: A size-segregated particle dry deposition scheme for an atmospheric aerosol module, Atmospheric Environment, 35, 549–560, https://doi.org/10.1016/s1352-2310(00)00326-5, 2001.

Table 2. Scorecard for the relative performance of the e-suite versus the performance of the o-suite against observations. Meaning of the "relative score" symbols: (++) e-suite performs significantly better than the o-suite (+) e-suite shows small improvements, (n) (neutral) no significant difference between o-suite and e-suite, (-) score is somewhat degraded in the e-suite, (–) e-suite performs significantly worse than the o-suite. Remote: Remote Sensing from surface station. [1] Based on the average statistics of ACE-FTS, SAGE-III/ISS, OMPS-LP, Aura MLS and ozonesondes. [2] Based on data from a network of stations that were collected by FMI.

| Species	Reference	Class	Type	Region	Relative Score
AOD	AERONET	Remote	Column	Global	+
AOD	AERONET	Remote	Column	Europe	n
AOD	AERONET	Remote	Column	North America	+
AOD	AERONET	Remote	Column	East Asia	+
AOD coarse	AERONET SDA	Remote	Column	Sahara	n
AOD coarse	AERONET SDA	Remote	Column	N. Atlantic & Mediterranean	+
AOD coarse	AERONET SDA	Remote	Column	Middle East	-
AE	AERONET	Remote	Column	Global	+
AE	AERONET	Remote	Column	Europe	+
AE	AERONET	Remote	Column	North America	+
AE	AERONET	Remote	Column	East Asia	+
AE	AERONET	Remote	Column	Sahara	n
AE	AERONET	Remote	Column	Middle East	-
PM10	AIRBASE	In-situ	Surface	Europe	n
PM10	CNEMC	In-situ	Surface	East Asia	-
PM10	AIRNOW	In-situ	Surface	North America	+
PM2.5	AIRBASE	In-situ	Surface	Europe	n
PM2.5	CNEMC	In-situ	Surface	East Asia	-
PM2.5	AIRNOW	In-situ	Surface	North America	+
O_3	GAW, ESRL, IASOA	In-situ	Surface	Global	n
O_3	AIRBASE	In-situ	Surface	Europe	n
O_3	CNEMC	In-situ	Surface	East Asia	+
O_3	AIRNOW	In-situ	Surface	North America	+
O_3	IAGOS	Aircraft	Tropospheric Profiles	Global	n
O_3	Sondes	Sondes	Tropospehric Profiles	Global	n
O_3	NDACC	Remote	1-50 hPa	Global	n
O_3	REF[1]	Satellite	1-10 hPa	Global	-
O_3	REF[1]	Satellite	10-200 hPa	Tropics	++
O_3	REF[1]	Satellite	10-200 hPa	Global	+
O_3	IASI	Satellite	Column	Global	+
CO	GAW	In-situ	Surface	Global	n
CO	AIRBASE	In-situ	Surface	Europe	+
CO	CNEMC	In-situ	Surface	East Asia	-
CO	NDACC FTIR	Remote	Tropospheric Profiles	Global	+
CO	NDACC FTIR	Remote	Stratospheric Profiles	Global	+
CO	IAGOS	Aircraft	Tropospheric Profiles	Global	+
CO	IASI	Satellite	Column	Global	+
CO	MOPITT	Satellite	Column	Global	-
NO_2	AIRBASE	In-situ	Surface	Europe	+
NO_2	CNEMC	In-situ	Surface	East Asia	+
NO_2	AIRNOW	In-situ	Surface	North America	n
NO_2	TROPOMI	Satellite	Tropospheric Column	Global	+
NO_2	TROPOMI	Satellite	Stratospheric Column	Global	++
SO_2	AIRBASE	In-situ	Surface	Europe	+
SO_2	CNEMC	In-situ	Surface	East Asia	+
HCHO	TROPOMI	Satellite	Tropospheric Column	Global	-
UV	REF[2]	In-situ	Surface	Global	n
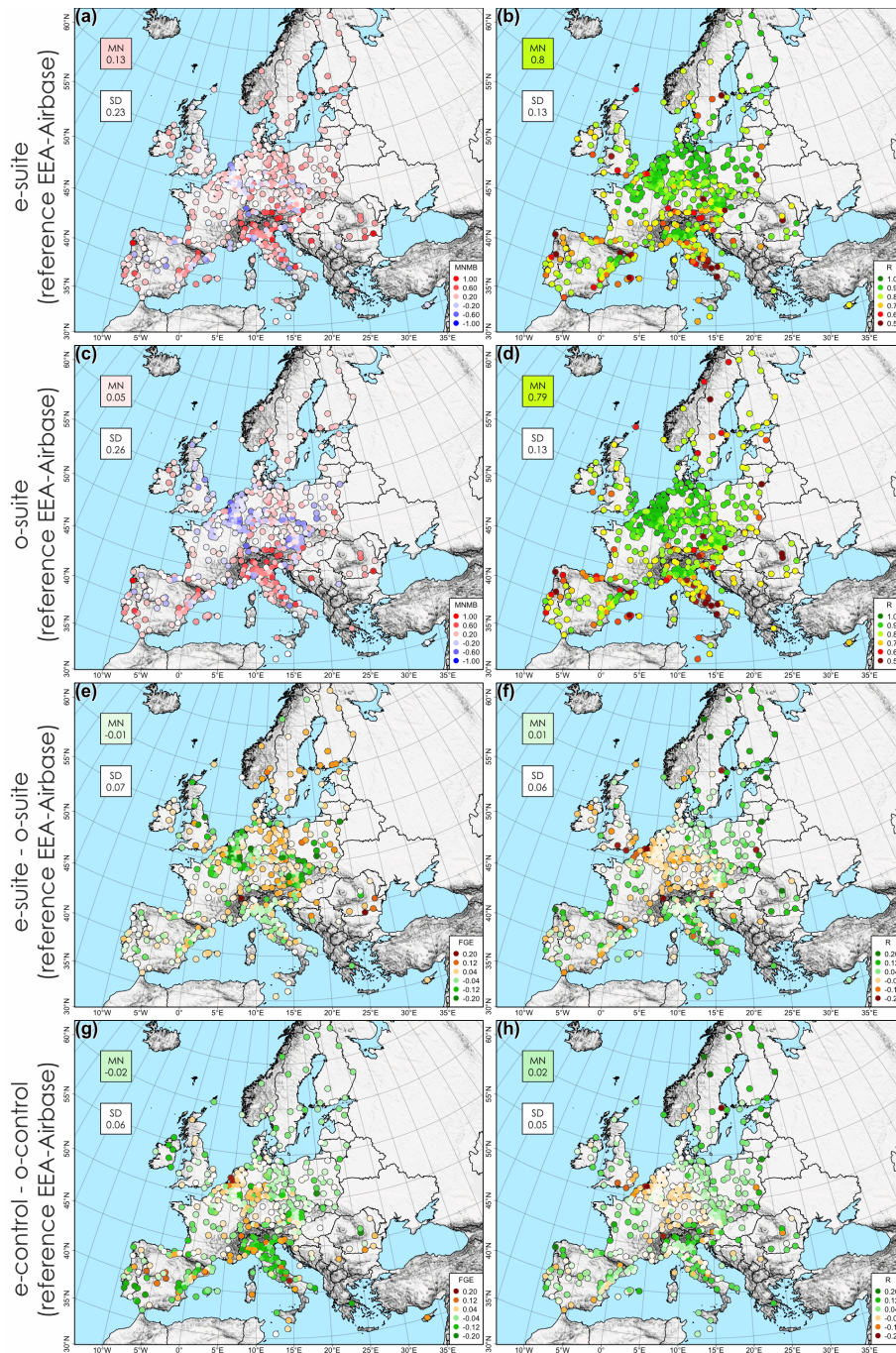
Figure 1. Spatial distribution of the surface O$_3$ evaluation over Europe, for the e-suite minus EEA-Airbase observations (first row, left: MNMB, right: R), the o-suite minus observations (second row, left: MNMB, right: R), the e-suite minus the o-suite differences (third row, left: FGE, right: R) and the e-control minus the o-control differences (fourth row, left: FGE, right: R) for the period 2023-10-01 to 2023-06-27. The mean (MN) and standard deviation (SD) for all station is depicted for each map.
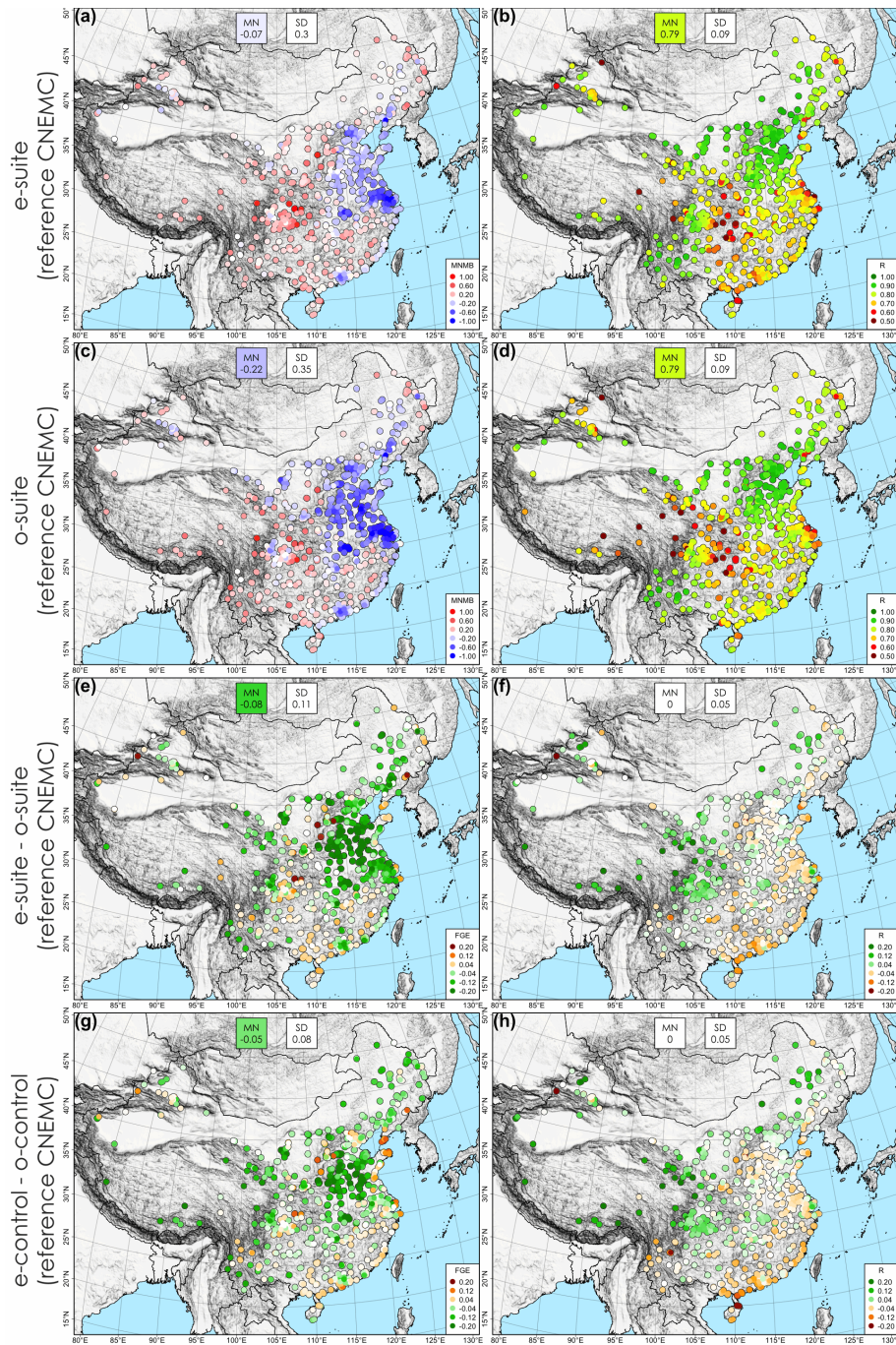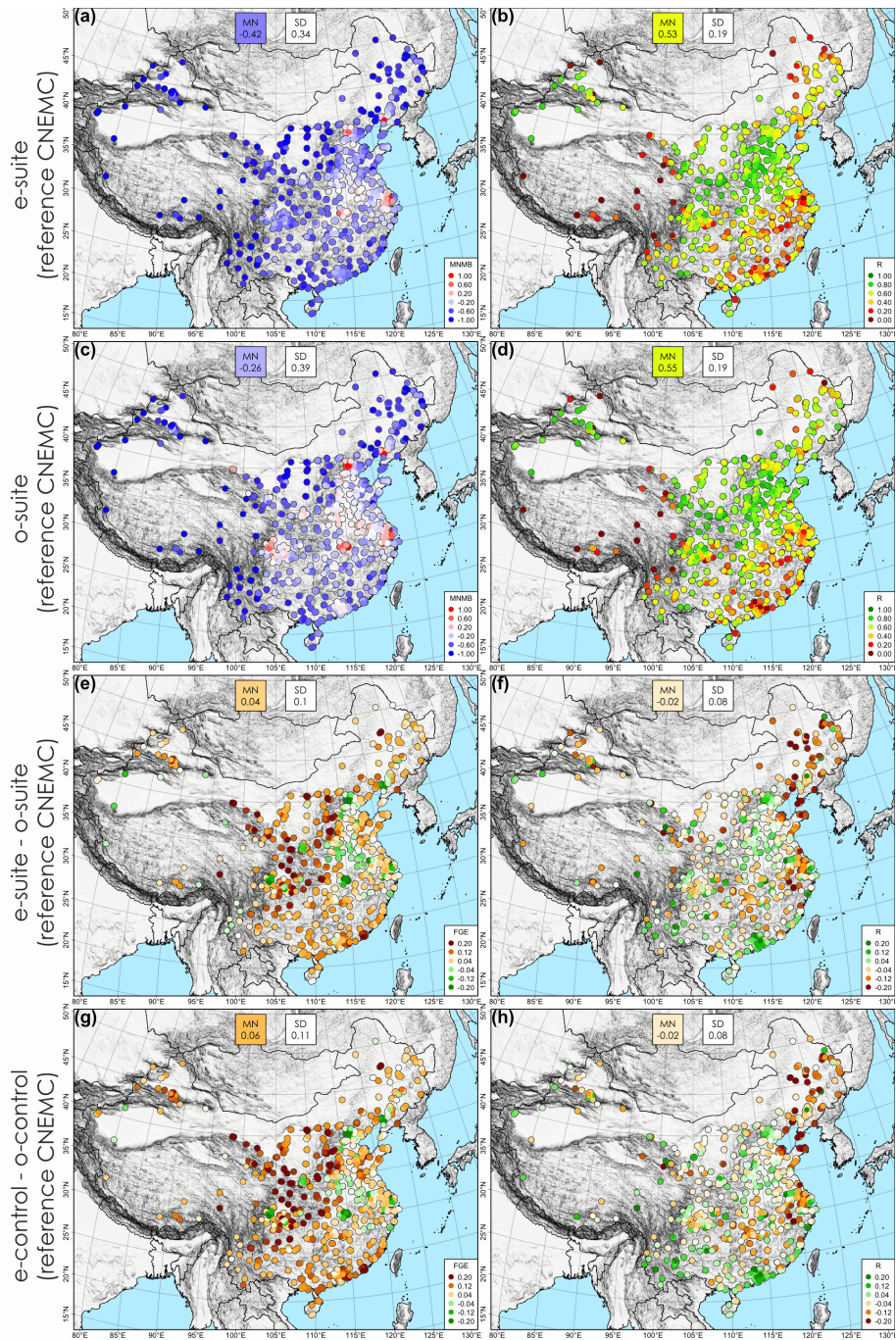
Figure 2. Spatial distribution of the O$_3$ evaluation over China, for the e-suite minus CNEMS observation (first row, left: MNMB, right: R), the o-suite miinus observations (second row, left: MNMB, right: R), the e-suite minus the o-suite differences (third row, left: FGE, right: R) and the e-control minus the o-control differences (fourth row, left: FGE, right: R) for the period 2023-10-01 to 2023-06-27. The mean (MN) and standard deviation (SD) for all station is depicted for each map.
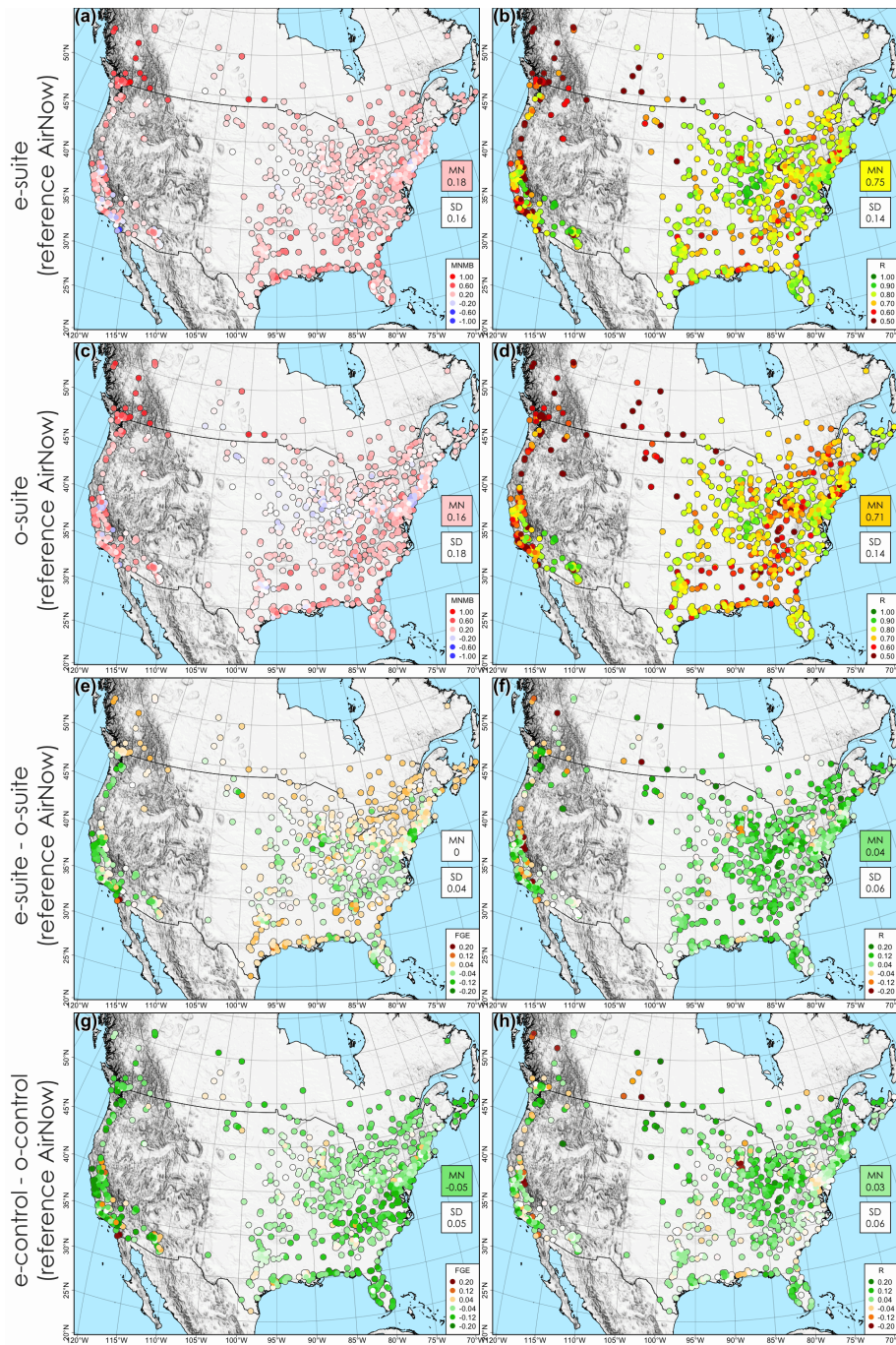
Figure 3. Spatial distribution of the O_3 evaluation over the USA and Canada, for the e-suite minus AirNow observations (first row, left: MNMB, right: R), the o-suite minus observations (second row, left: MNMB, right: R), the e-suite minus the o-suite differences (third row, left: FGE, right: R) and the e-control minus the o-control differences (fourth row, left: FGE, right: R) for the period 2023-10-01 to 2023-06-27. The mean (MN) and standard deviation (SD) for all station is depicted for each map.
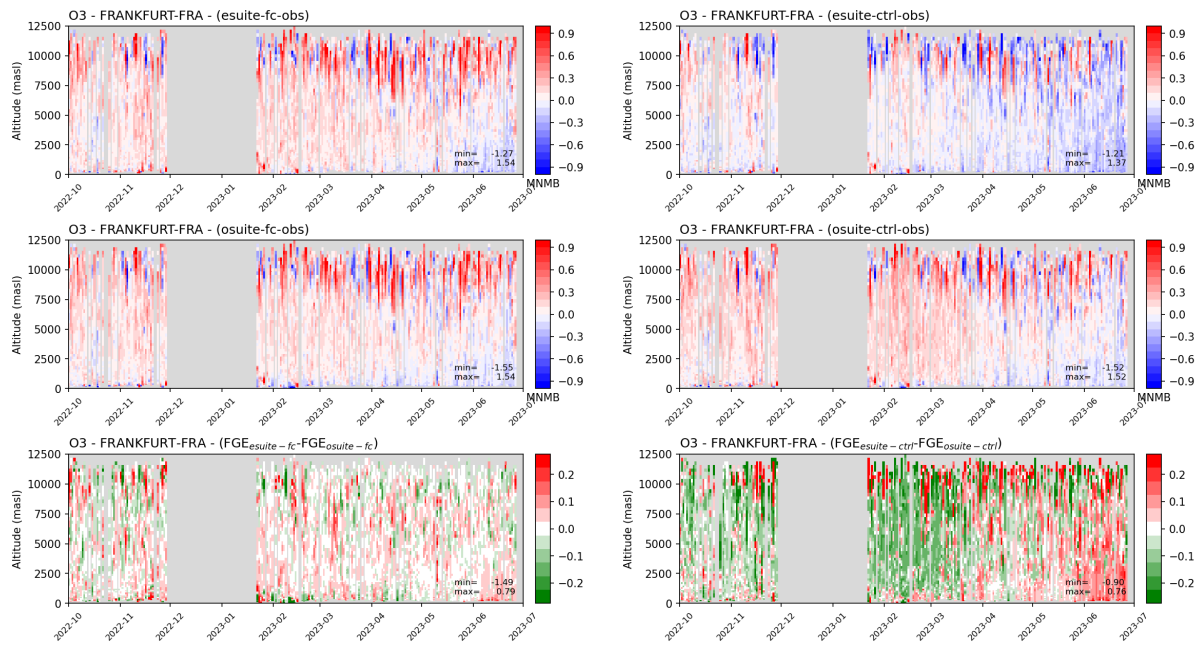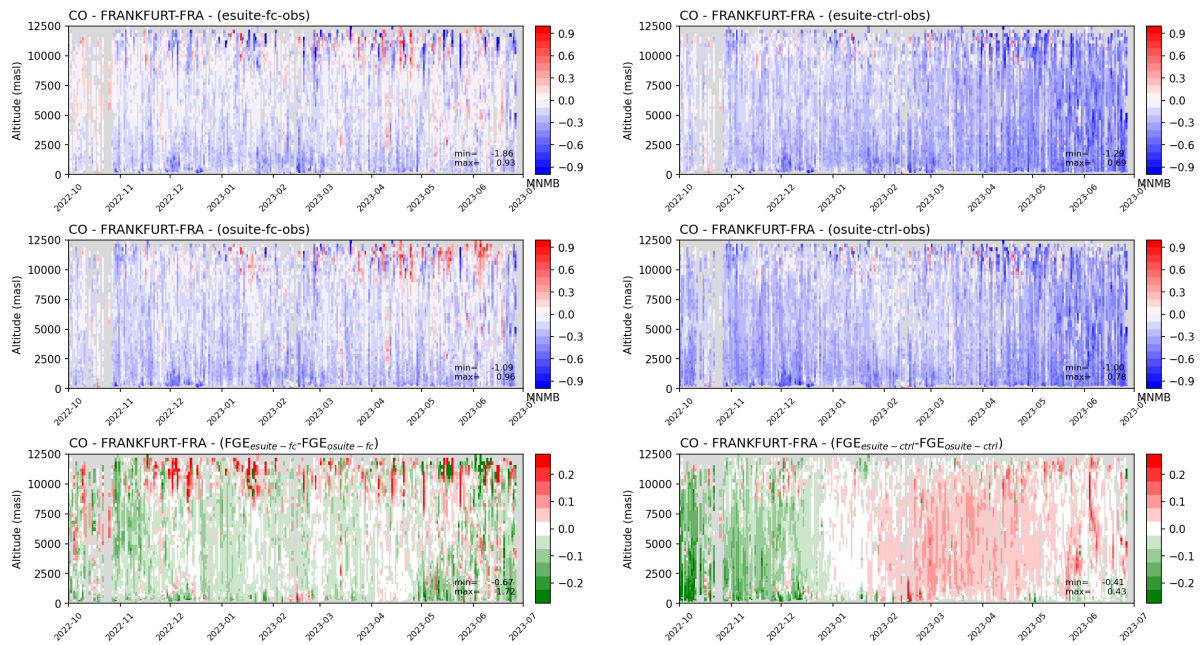
Figure 4. Ozone comparisons using aircraft profile observations from IAGOS (http://www.iagos.org). Time series of modified normalized differences CAMS-IAGOS in the daily profiles of ozone at Frankfurt between October 2022 and 27 June 2023 for the e-suite (top-left), the o-suite (middle-left) and their respective control runs (right). The fractional gross error differences between the e-suite and the o-suite are shown in the bottom row.
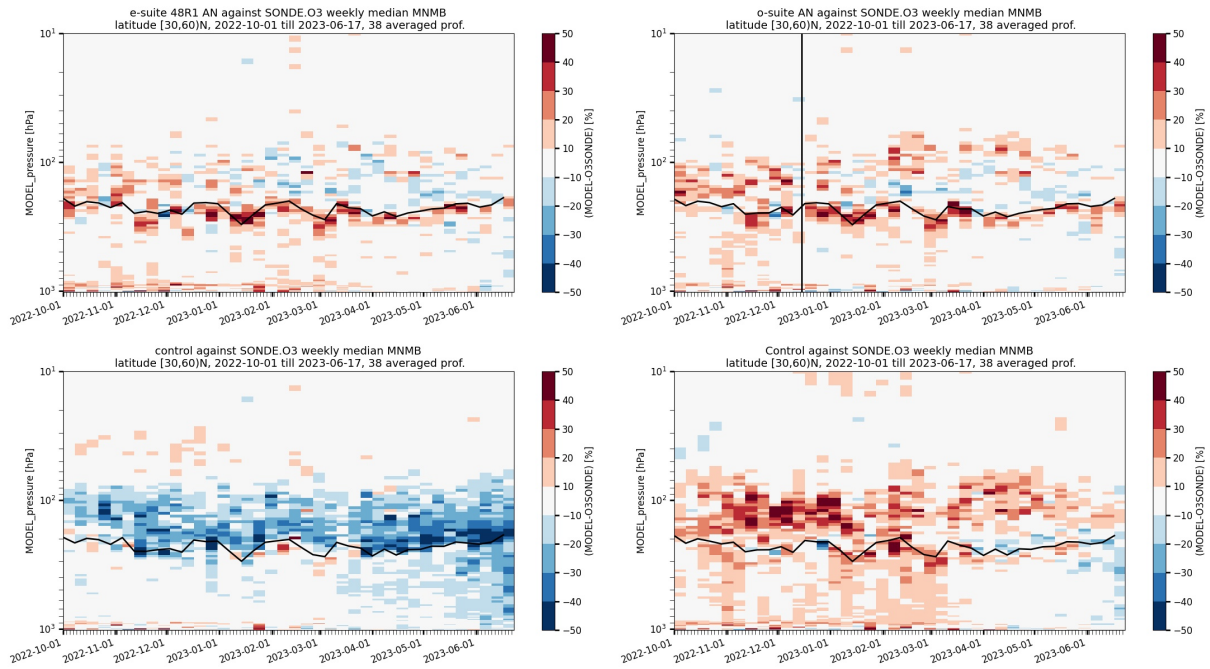
Figure 5. Comparisons against ozonesondes. Time-pressure curtain plot of ozone profile MNMB for the e-suite analysis (top-left), the o-suite analysis (top-right), the e-suite control run (bottom-left) and o-suite control run (bottom-right) against sonde profiles for the northern hemisphere midlatitudes. The horizontal black line represents the tropopause. The vertical black line in the o-suite plot indicates the 15 December change in the background error covariance in Cy47R3.
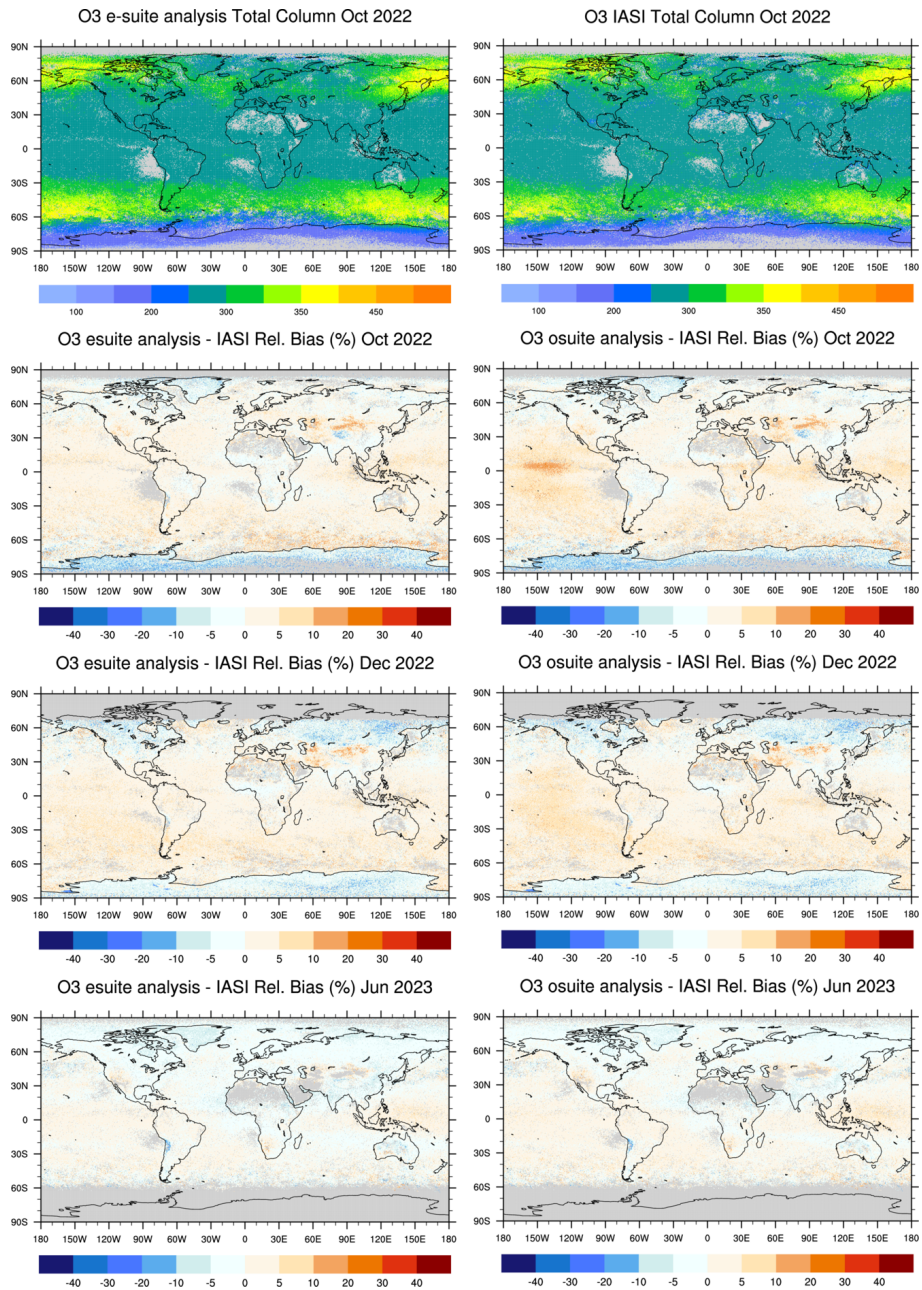
Figure 6. Global maps of monthly mean total column ozone (Dobson Unit) compared with satellite observations from IASI. The plot shows the e-suite result (top left) and the IASI observations (top right) for October 2022, below the relative bias of the e-suite (left column) and the relative bias of the o-suite (right column) with respect to IASI (%) for October 2022 (second row), December 2022 (third row) and June 2023 (bottom).
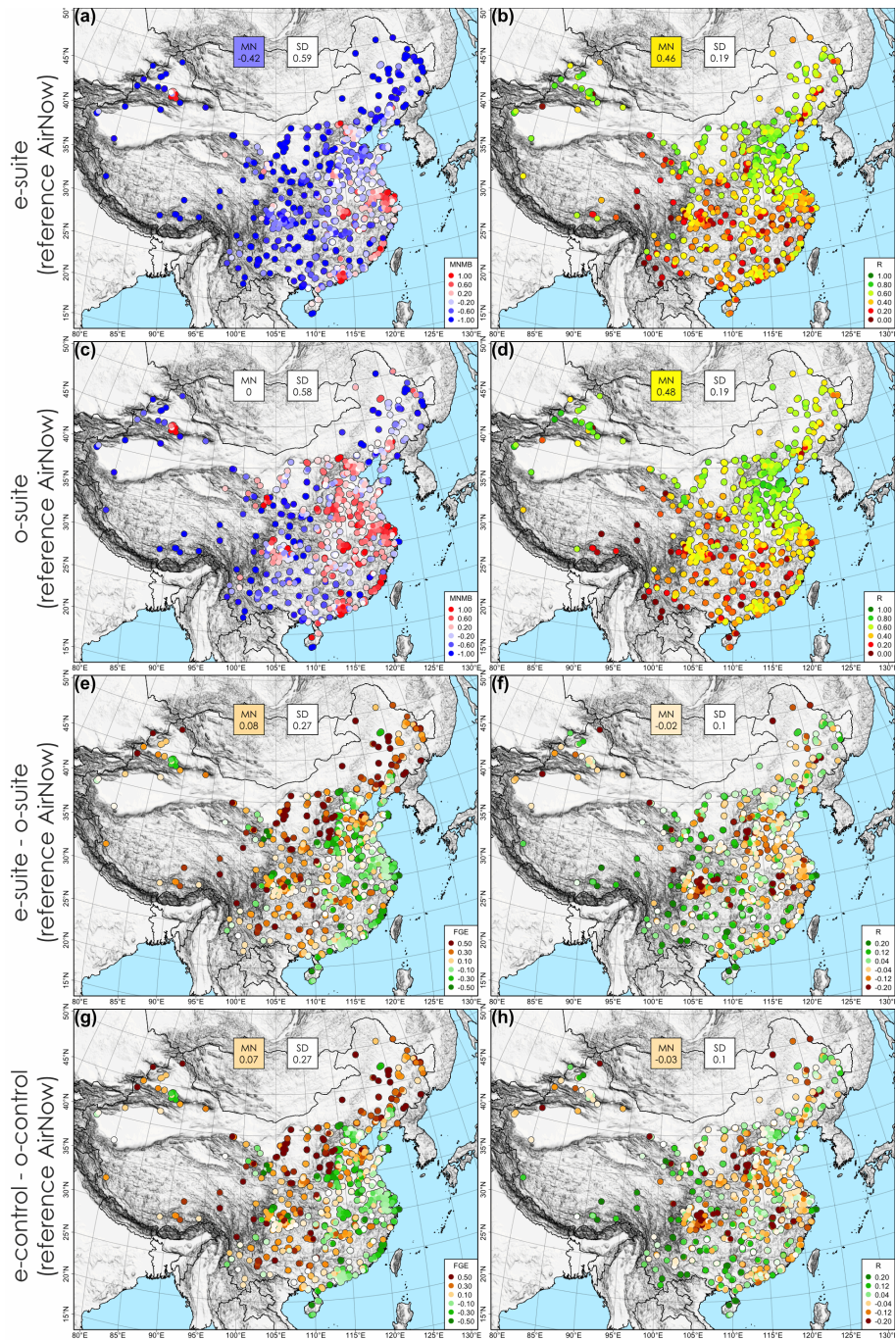
Figure 7. Spatial distribution of the CO surface comparisons over China, for the e-suite minus CNEMC observations (first row, left: MNMB, right: R), the o-suite minus observations (second row, left: MNMB, right: R), the e-suite minus the o-suite differences (third row, left: FGE, right: R) and the e-control minus the o-control differences (fourth row, left: FGE, right: R) for the period 2023-10-01 to 2023-06-27. The mean (MN) and standard deviation (SD) for all station is depicted for each map.

Figure 8. CO comparisons using aircraft profile observations from IAGOS (http://www.iagos.org). Time series of modified normalized differences CAMS-IAGOS in the daily profiles of ozone at Frankfurt between October 2022 and 27 June 2023 for the e-suite (top-left), the o-suite (middle-left) and their respective control runs (right). The fractional gross error differences between the e-suite and the o-suite are shown in the bottom row.
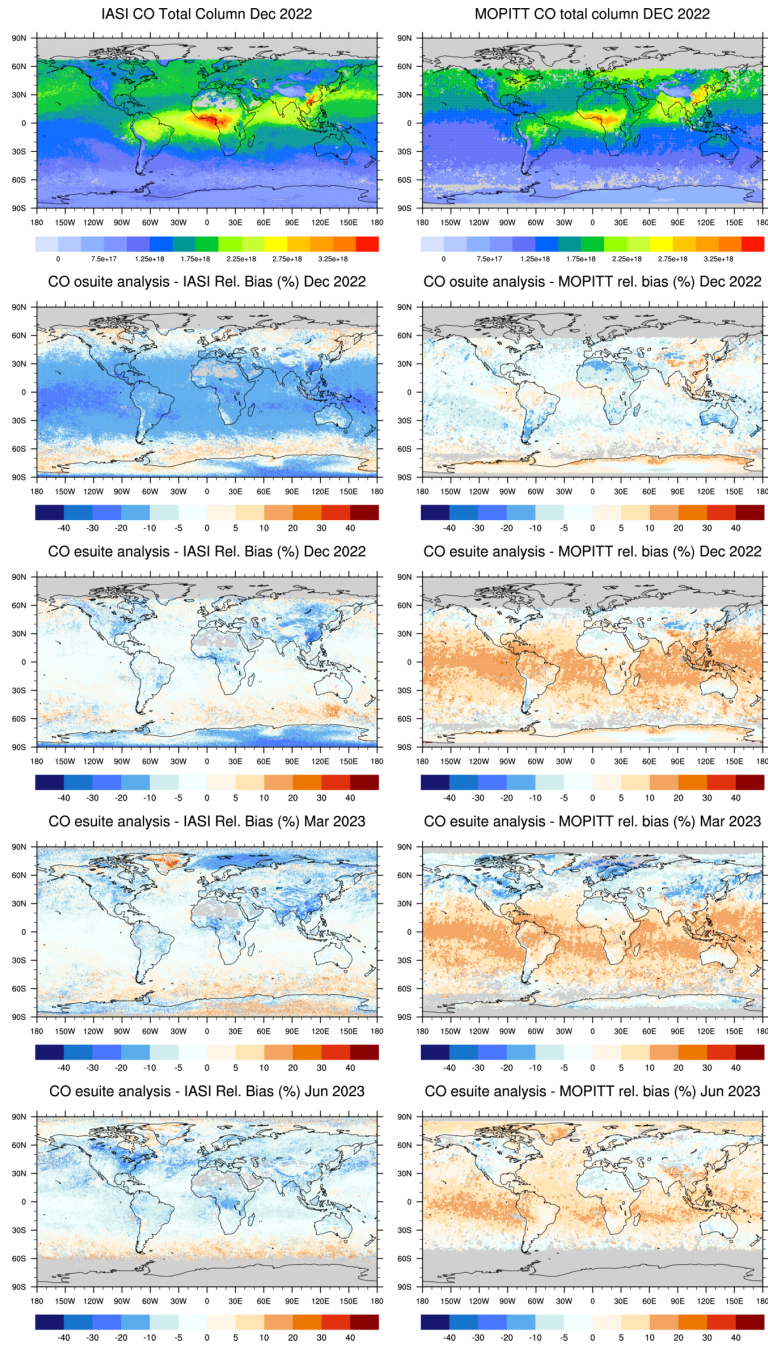
Figure 9. Global maps of monthly mean total column CO comparing satellite observations from IASI (left column) with MOPITT (right column) validation including the satellite observation (first row), the relative bias of the o-suite result with respect to the satellite data (second row), and the relative bias of the e-suite result (third row) for Dec 2022, as well as the e-suite relative bias for March and June 2023 (fourth and fifth row, respectively).

38
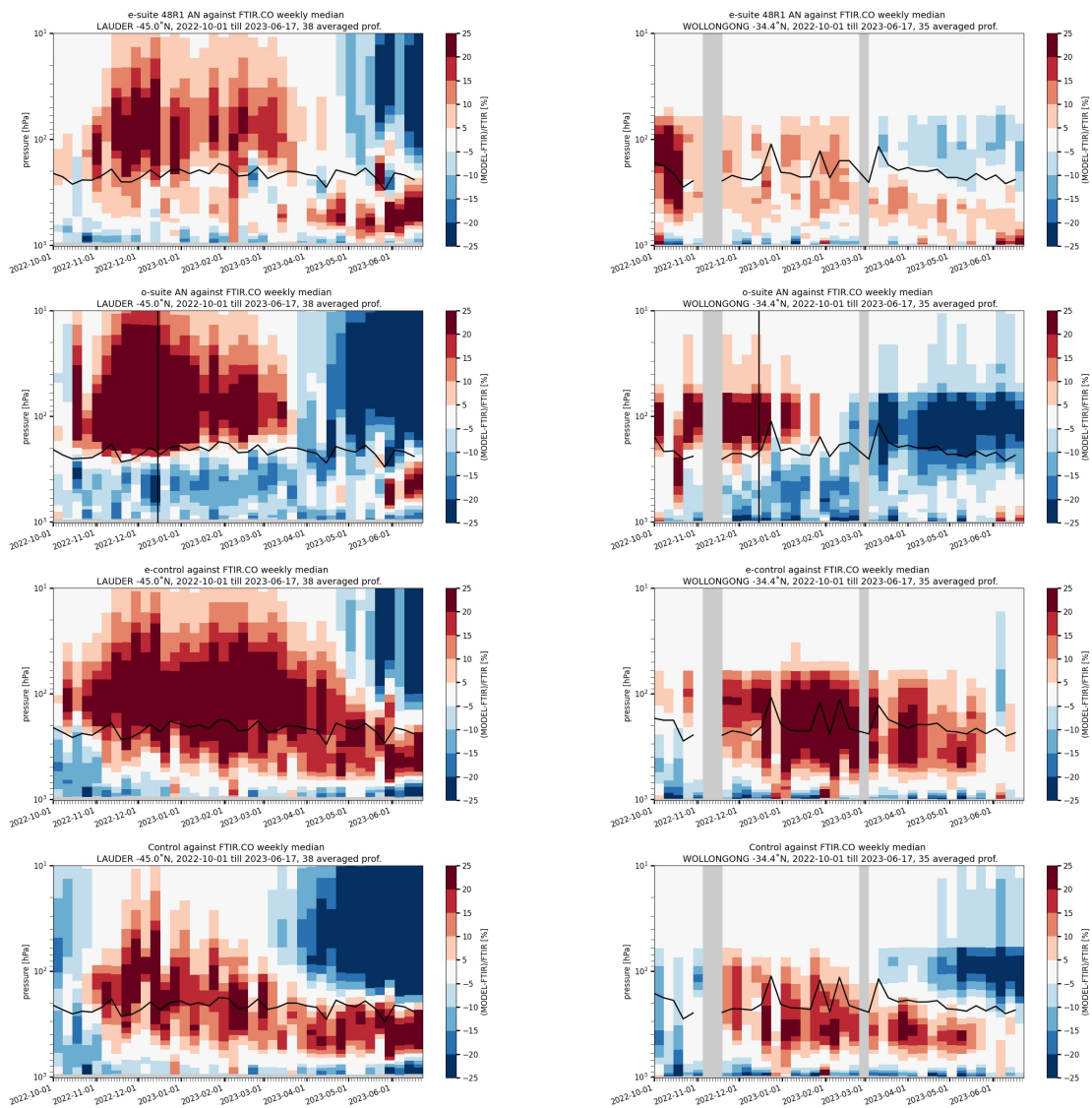
Figure 10. Curtain plots of the CO profile relative difference of the CAMS products compared to FTIR observations from the NDACC network for the two southern hemispheric stations Lauder (left) and Wollongong (right). Shown are the differences with the e-suite (top row), o-suite (second row), e-control (third row) and o-control (bottom row). Model profiles are smoothed with the FTIR averaging kernels. The horizontal black line is the tropopause. The vertical black line indicates 15 December, when the change in the background error covariance was implemented.
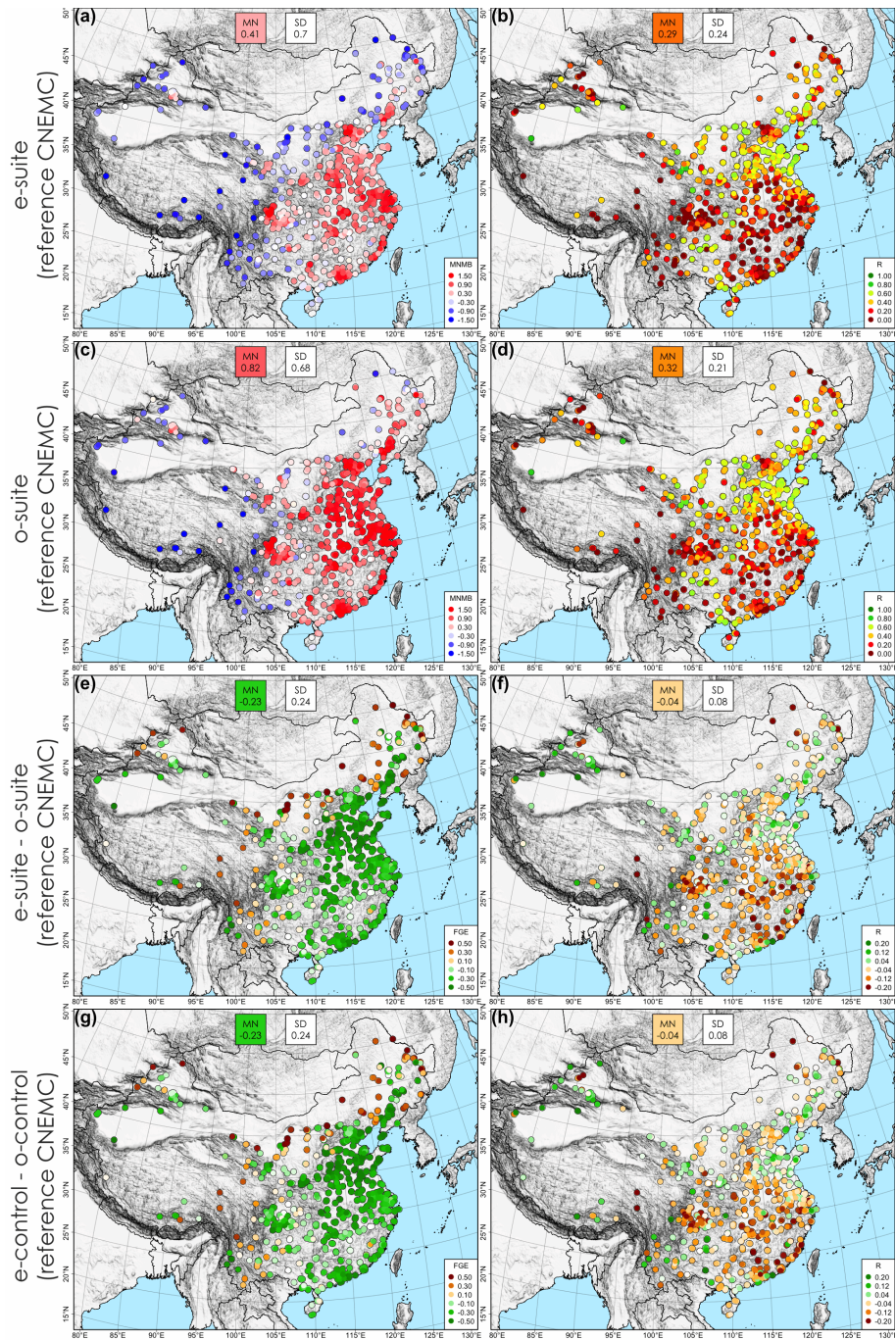
Figure 11. Spatial distribution of the NO$_2$ surface comparisons over China, for the e-suite minus CNEMC observations (first row, left: MNMB, right: R), the o-suite minus observations (second row, left: MNMB, right: R), the e-suite minus the o-suite differences (third row, left: FGE, right: R) and the e-control minus the o-control differences (fourth row, left: FGE, right: R) for the period 2023-10-01 to 2023-06-27. The mean (MN) and standard deviation (SD) for all station is depicted for each map.
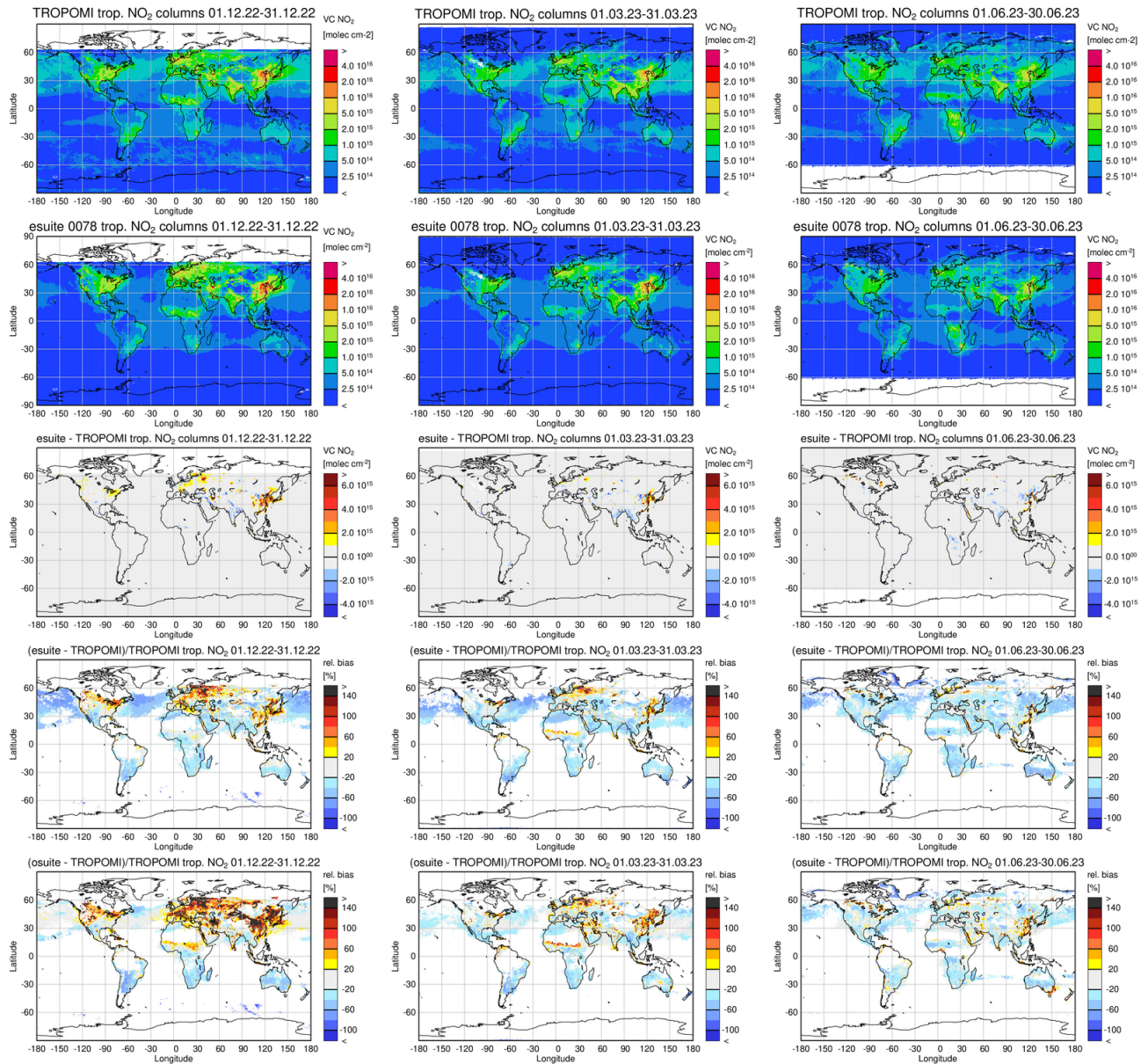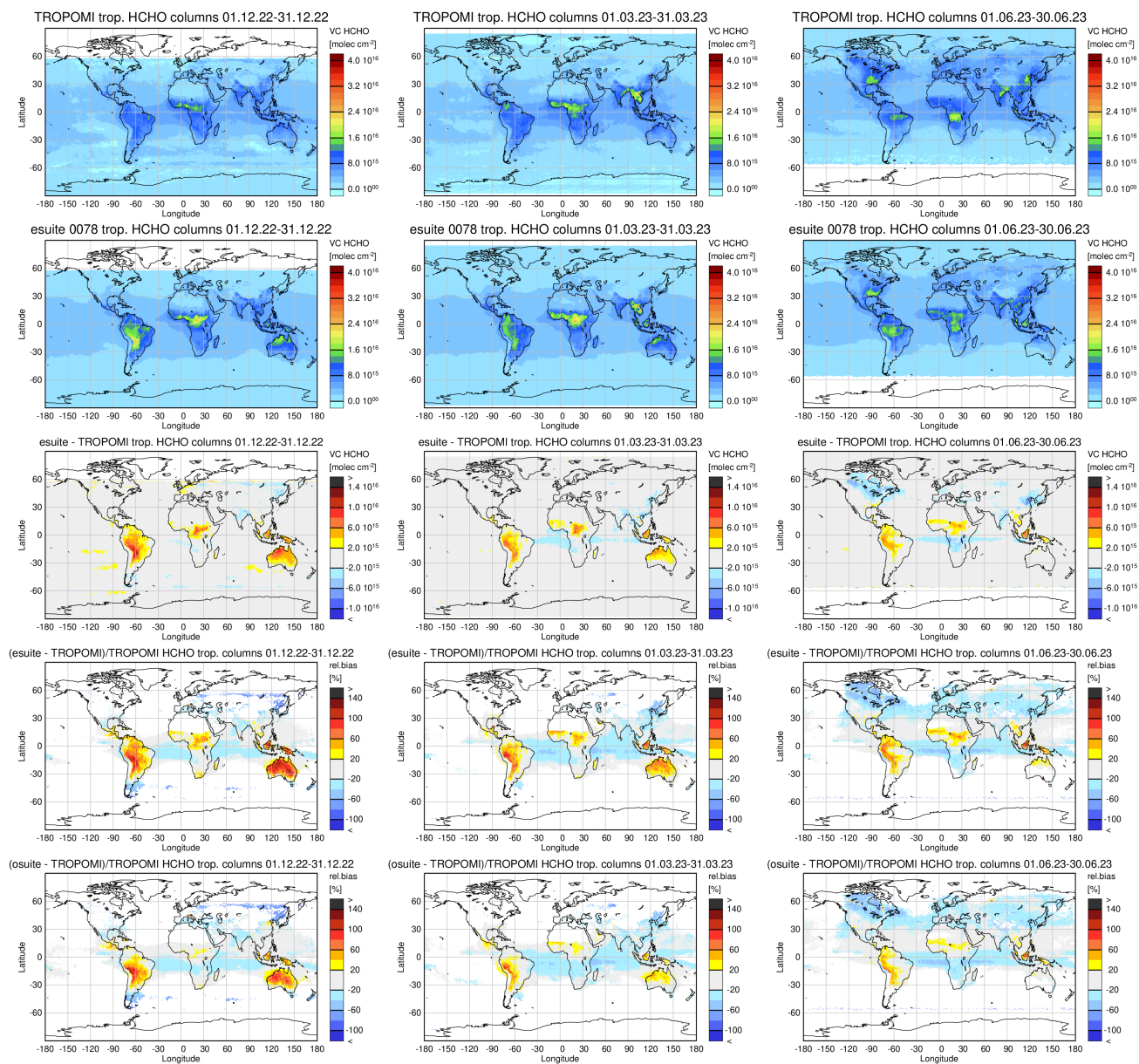
Figure 12. Monthly mean global maps of tropospheric NO_2 column densities for TROPOMI satellite observations (first row), the e-suite (second row), the difference between e-suite and satellite (third row), the relative difference between e-suite and satellite (fourth row) and the relative difference between o-suite and satellite (fifth row) for December 2022 (left column), March 2023 (middle column) and June 2023 (right column). Units: 1e15 molecules cm^{-2}. Note that for the relative bias the regions with background values below 5x10^{14} molec. cm^{-2} are not included in the analysis.

Figure 13. Spatial distribution of the SO$_2$ surface comparisons over China, for the e-suite minus CNEMC observations (first row, left: MNMB, right: R), the o-suite minus observations (second row, left: MNMB, right: R), the e-suite minus the o-suite differences (third row, left: FGE, right: R) and the e-control minus the o-control differences (fourth row, left: FGE, right: R) for the period 2023-10-01 to 2023-06-27. The mean (MN) and standard deviation (SD) for all station is depicted for each map.

Figure 14. Monthly mean global maps of tropospheric HCHO column densities for TROPOMI satellite observations (first row), the e-suite (second row), the difference between e-suite and satellite (third row), the relative difference between e-suite and satellite (fourth row) and the relative difference between o-suite and satellite (fifth row) for December 2022 (left column), March 2023 (middle column) and June 2023 (right column). Units: 1e15 molecules cm^{-2}. Regions with mean background values below 3×10^{15} molec/cm2 are excluded from the analysis (white areas).
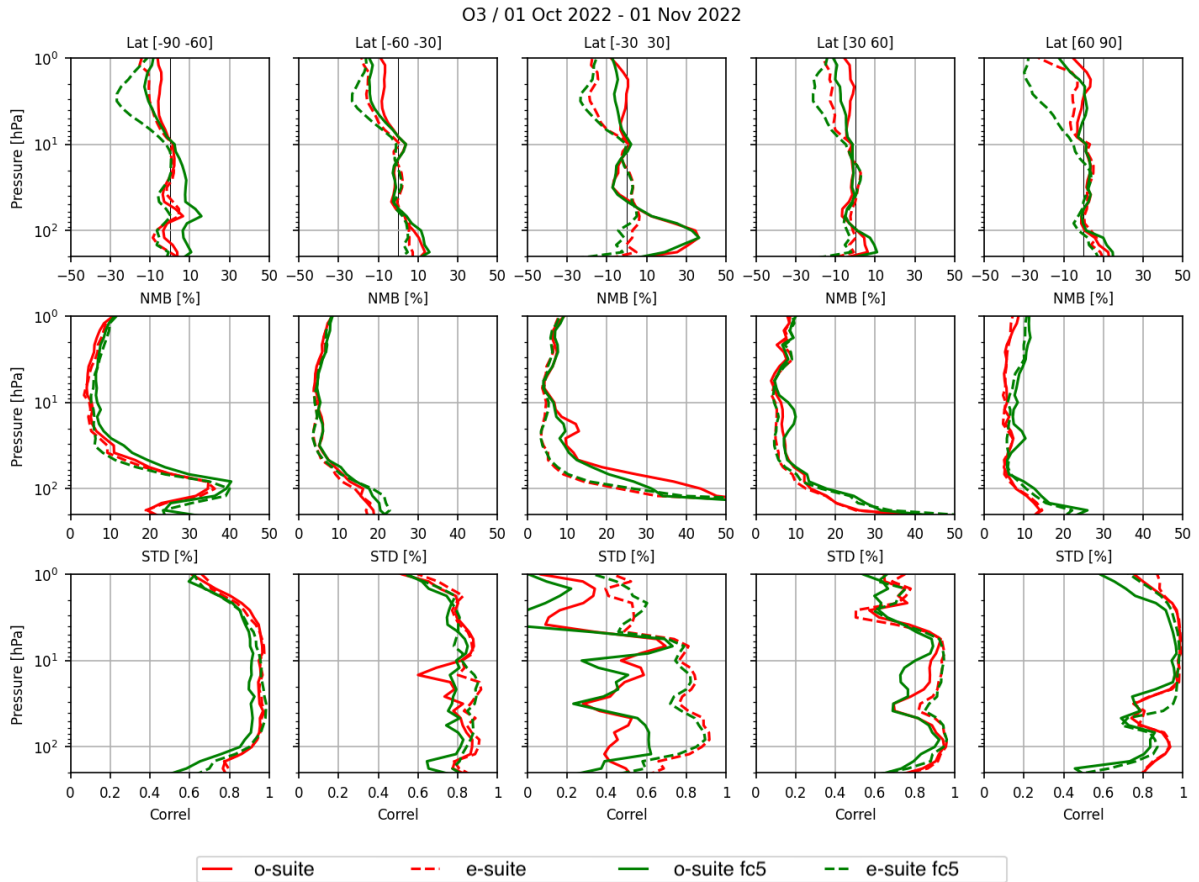
Figure 15. The e-suite and o-suite compared to a Multi-Instrument-Mean (MIM), consisting of observed ozone profiles from ACE-FTS v4.1, Aura-MLS v4.2, OMPS-LP v2.5, SAGE-III/ISS v5.2 and ozonesondes. Top row: normalised mean difference between the MIM ozone observed profiles and the o-suite analyses (solid red line), the o-suite 5th day forecast (solid green line), the e-suite analyses (dashed red line) and the e-suite 5th day forecast (dashed green line). The figure refers to the period October 2022, which is during the Antarctic ozone hole conditions. Five latitude bands are considered, from left to right: 90°S-60°S, 60°S-30°S, 30°S-30°N, 30°N-60°N and 60°N-90°N. The corresponding standard deviation of the differences and the correlation coefficient between observed profiles and the e-suite and o-suite runs is shown in the second and the third row respectively.
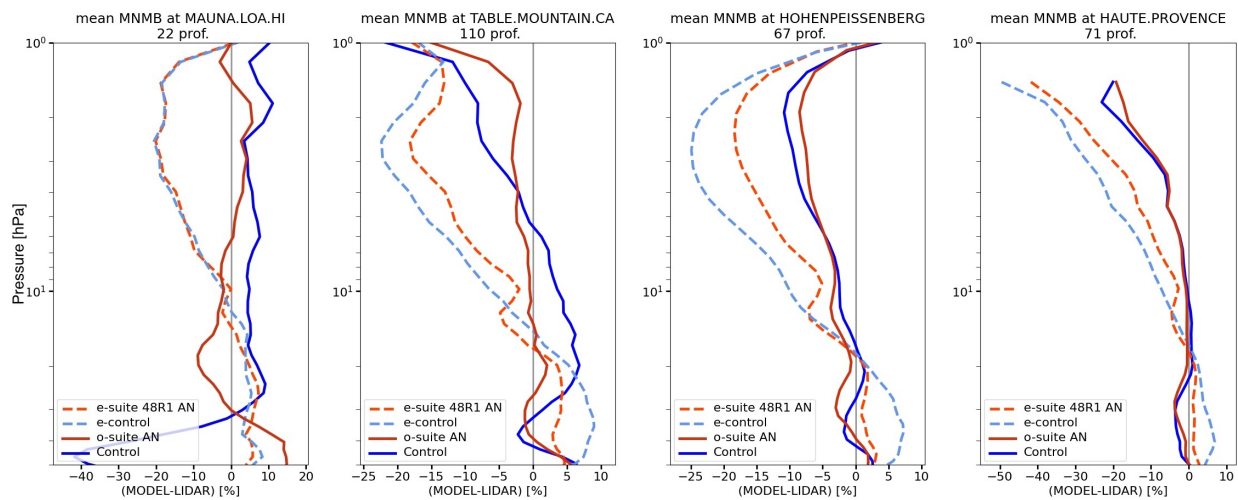
Figure 16. Mean ozone profile differences for e-suite (red dash), o-suite (red solid), e-suite control run (blue dash) and o-suite control run (blue solid) compared to stratospheric ozone lidar observations of four stations from the NDACC network.
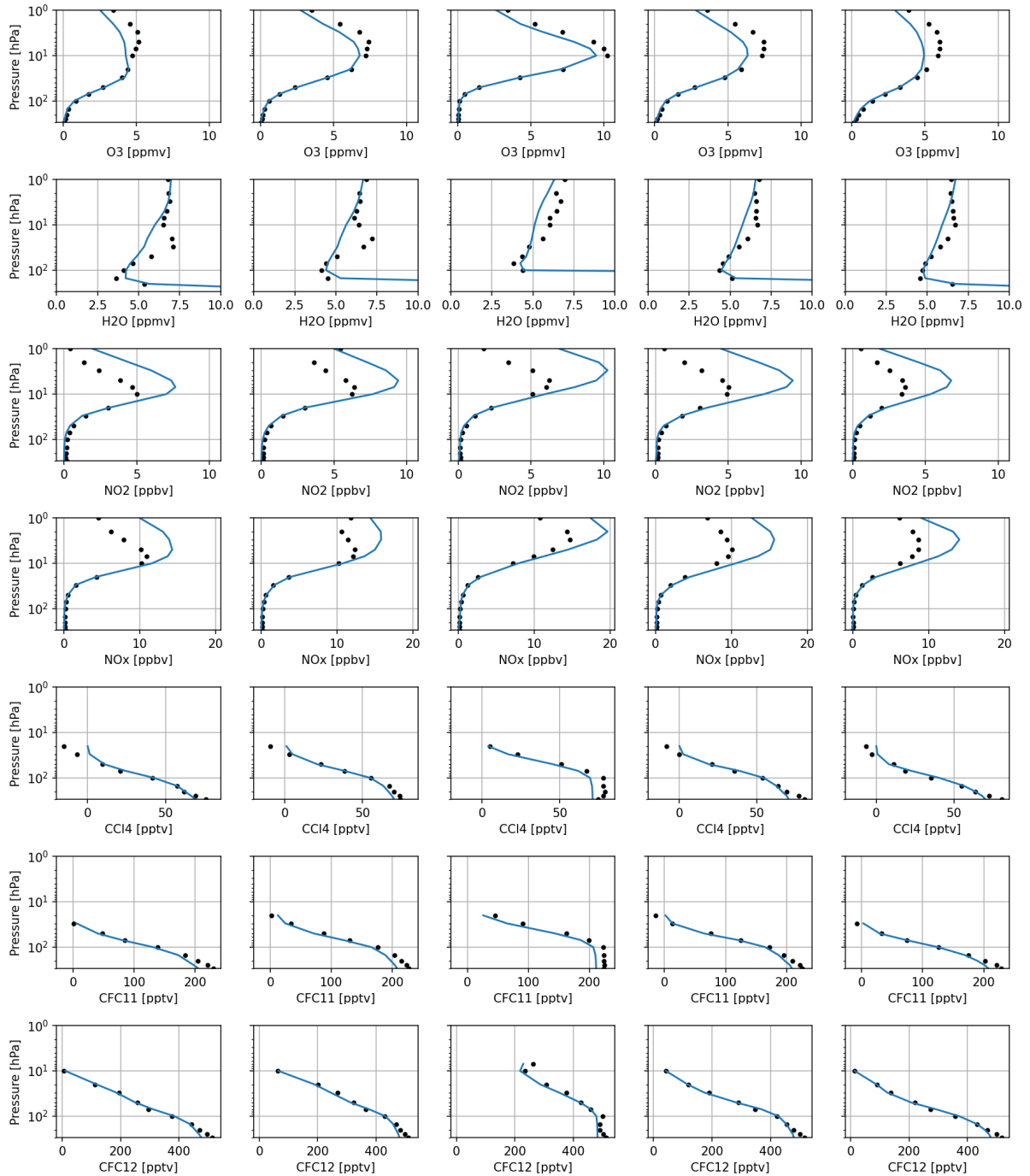
Figure 17. Comparison of O_3, H_2O, NO_2, NOx, CCl_4, CFC-11, CFC-12 from the e-suite first day forecast (blue lines) with ACE-FTS observations (black dots) between 1 Oct 2022 - 27 June 2023. Five latitude bands are considered, from left to right: 90°S-60°S, 60°S-30°S, 30°S-30°N, 30°N-60°N and 60°N-90°N.
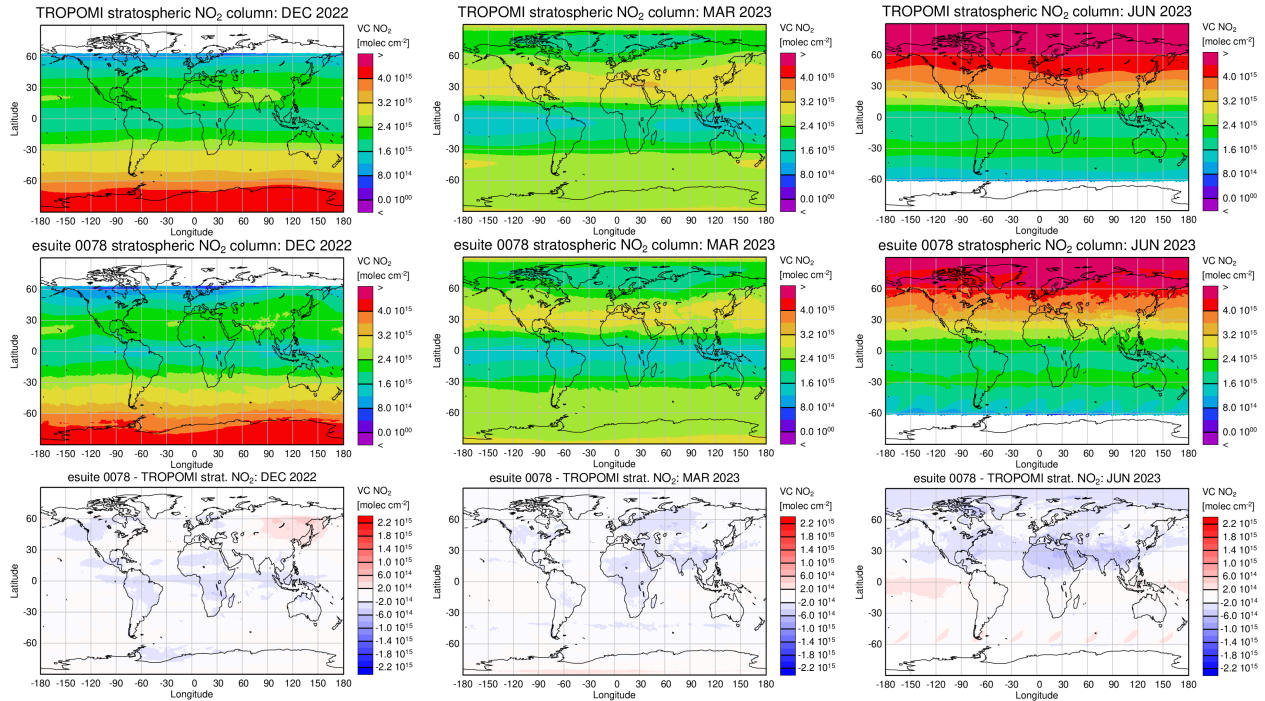
Figure 18. Monthly mean NO_2 stratospheric column amounts retrieved using TROPOMI observations (top) compared to the e-suite results (second row). The third row shows the differences between the e-suite and TROPOMI. Results are shown for December 2022 (left column), March 2023 (second column), and June 2023 (right column). The STREAM-B algorithm was used to estimate the stratospheric contribution to the total retrieved column (Eskes et al., 2023a).
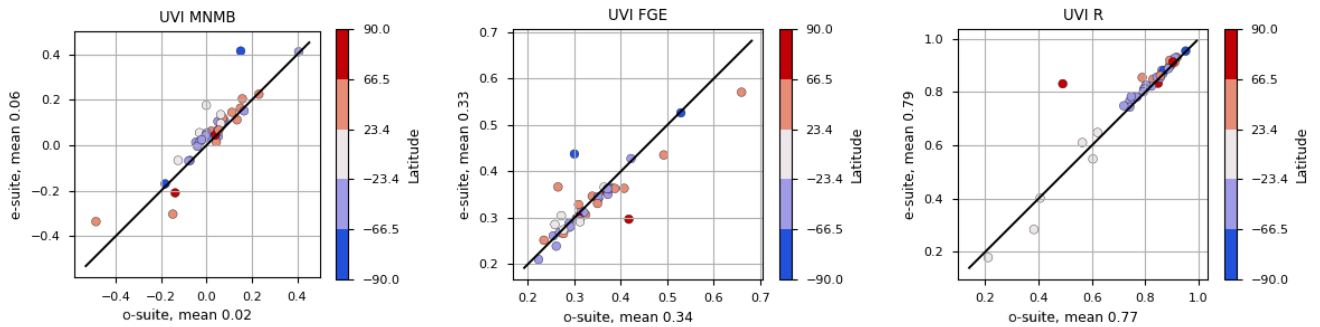
Figure 19. Hourly UV index values from the CAMS e-suite and o-suite evaluated against ground based UV measurements from 38 stations located in Europe, Israel, Thailand, Australia, New Zealand, and the Antarctic. Scatterplots of MNMB, FGE and R between measurements, and o-suite (Cy47R3, x-axis) and measurements, and e-suite (Cy48R1, y-axis). Each dot represents a single measurement station, either in the northern latitudes (red) or southern latitudes (blue). The time range is from 2022-10-01 to 2023-06-27.
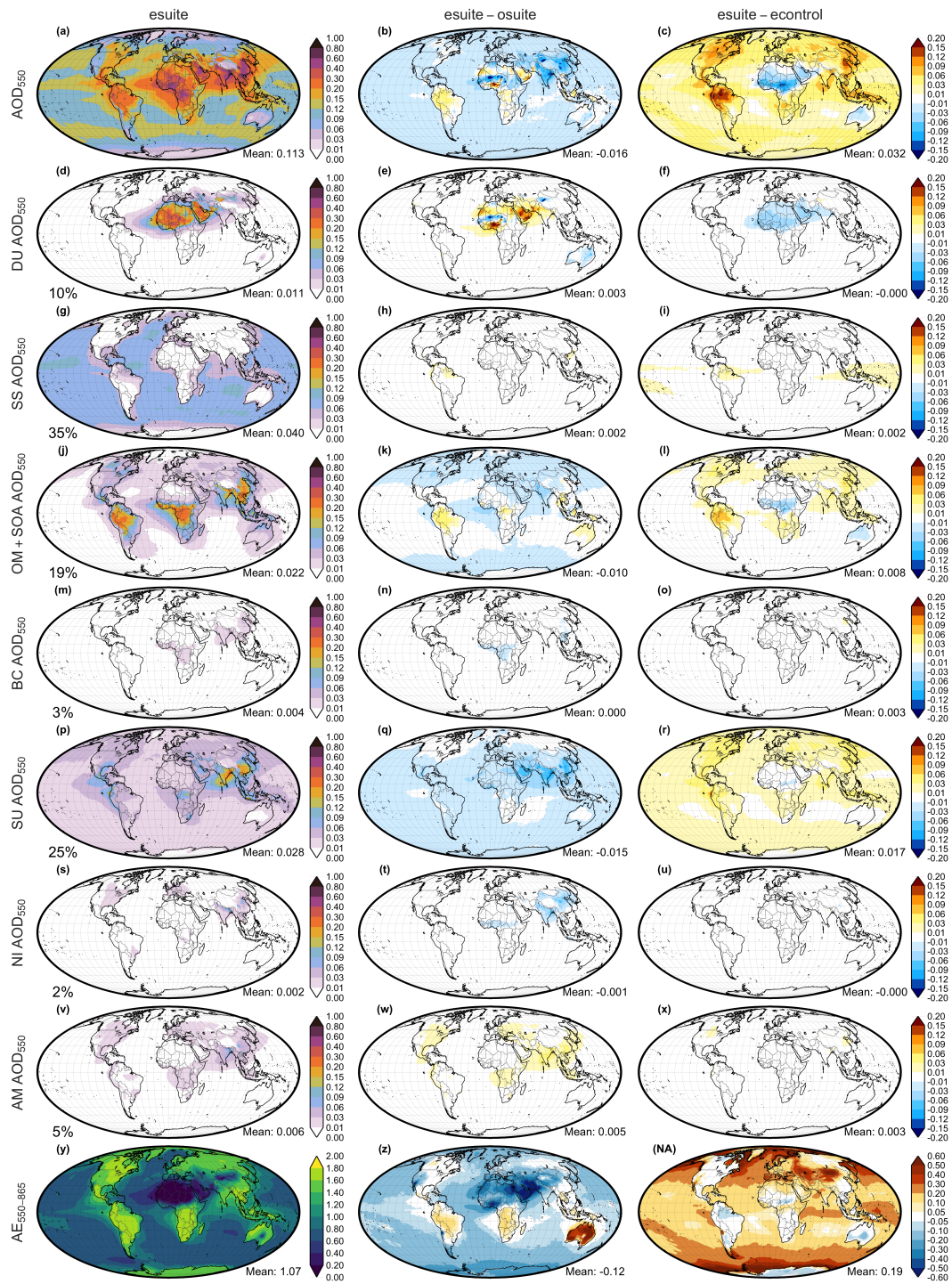
Figure 20. AOD (1st row), AOD for each species (2nd to 8th row) and Ångström Exponent (9th row) for e-suite (1st column), differences of e-suite - o-suite (2nd column) and differences of e-suite - e-control (3rd column) for the period 2022-10-01 to 2023-06-27. Species included are dust (DU), sea-salt (SS), organic matter plus secondary organic (OM+SOA), black carbon (BC), sulphate (SU), nitrate (NI) and ammonium (AM). Percentage at the bottom right corner of first column displays the relative contribution of each species optical depth to AOD.
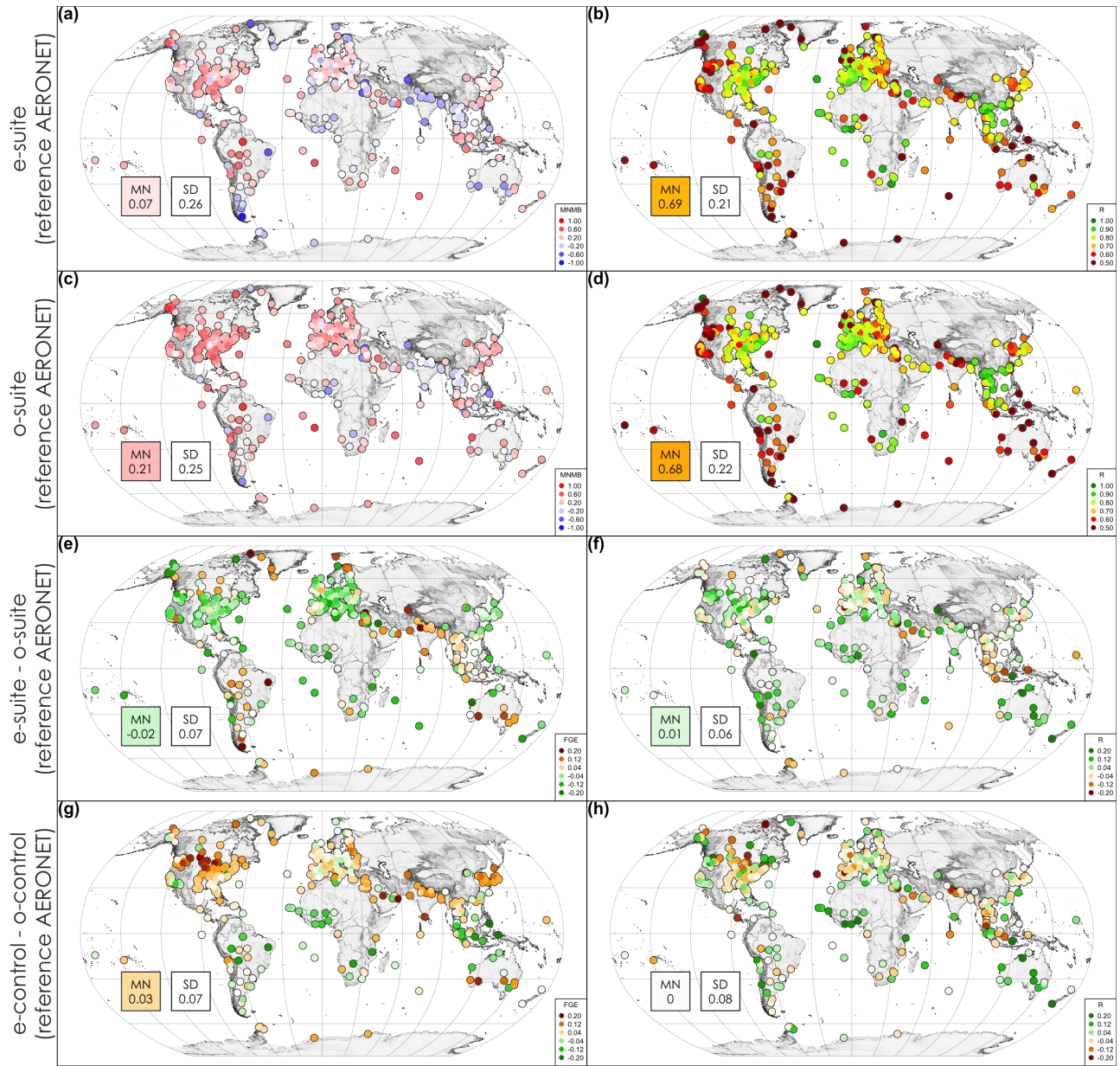
Figure 21. Spatial distribution of the daily Aerosol Optical Depth MNMB, FGE and R for the e-suite minus observations (first row), the o-suite minus observations (second row), the e-suite minus the o-suite differences (third row) and the e-control minus the o-control differences (fourth row) for the period 2023-10-01 to 2023-06-27 using as a reference AERONET v3 level 1.5. The mean (MN) and standard deviation (SD) for all station is depicted for each map.
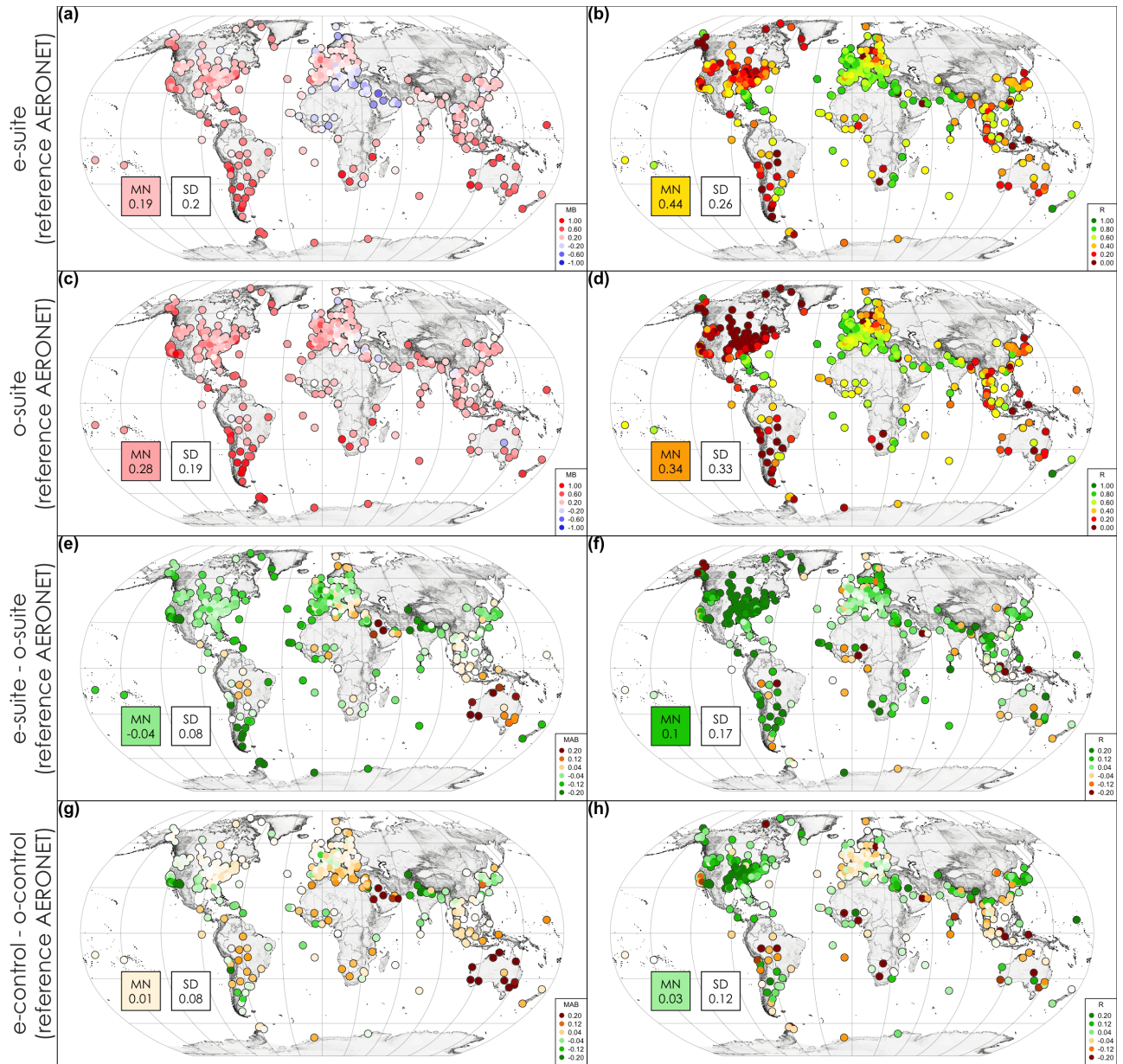
Figure 22. Spatial distribution of the daily Ångström Exponent MNMB, FGE and R for the e-suite minus observations (first row), the o-suite minus observations (second row), the e-suite minus the o-suite differences (third row) and the e-control minus the o-control differences (fourth row) for the period 2023-10-01 to 2023-06-27 using as a reference AERONET v3 level 1.5. The mean (MN) and standard deviation (SD) for all station is depicted for each map.
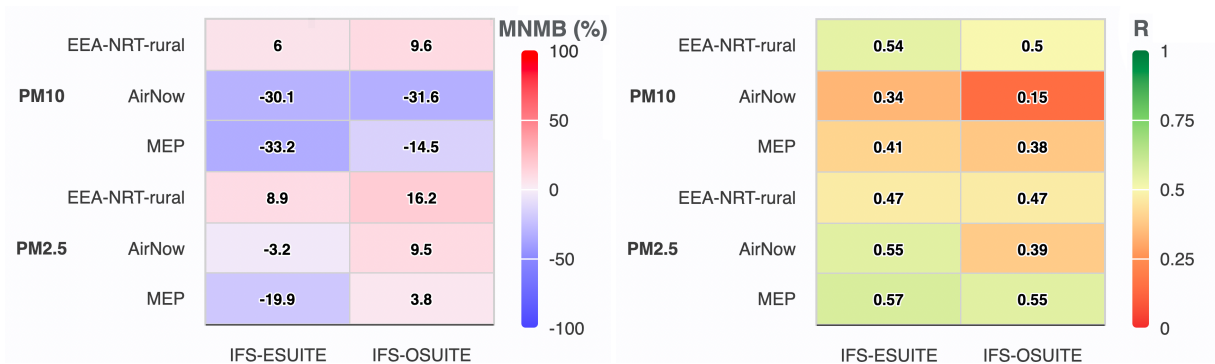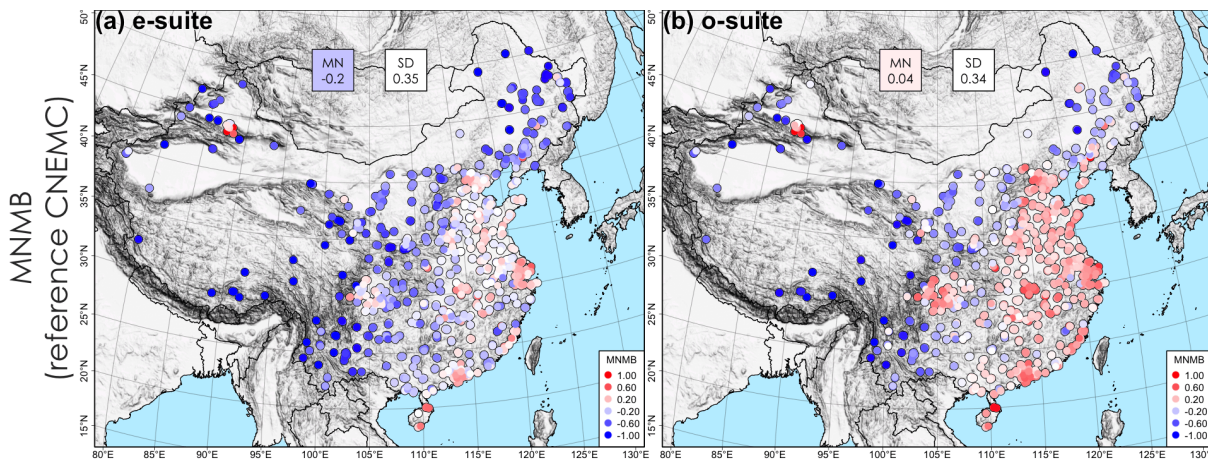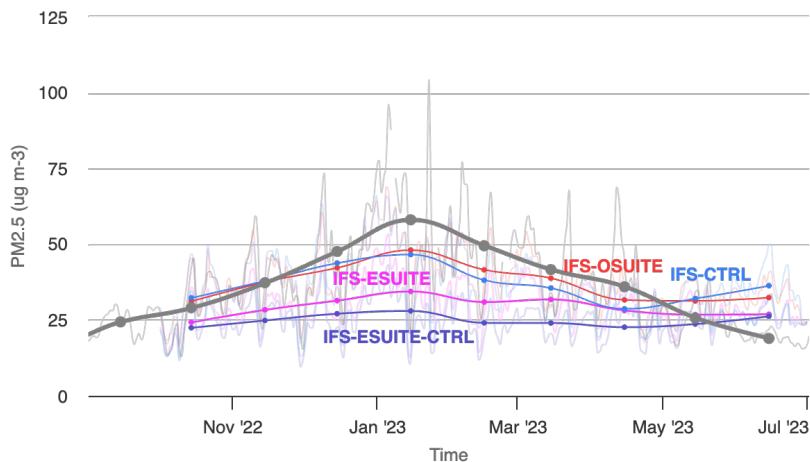
Figure 23. Modified Normal Mean Bias of CAMS minus observations (left) and correlation (right) of PM2.5 and PM10 based on EEA-NRT-rural (Europe), AirNow (North America) and MEP/CNEMC (East Asia) monitoring stations. The average timeseries for all stations over East Asia (second row) and the MNMB maps for o-suite and e-suite are also shown (third row). The mean (MN) and standard deviation (SD) for all station is depicted for each map.
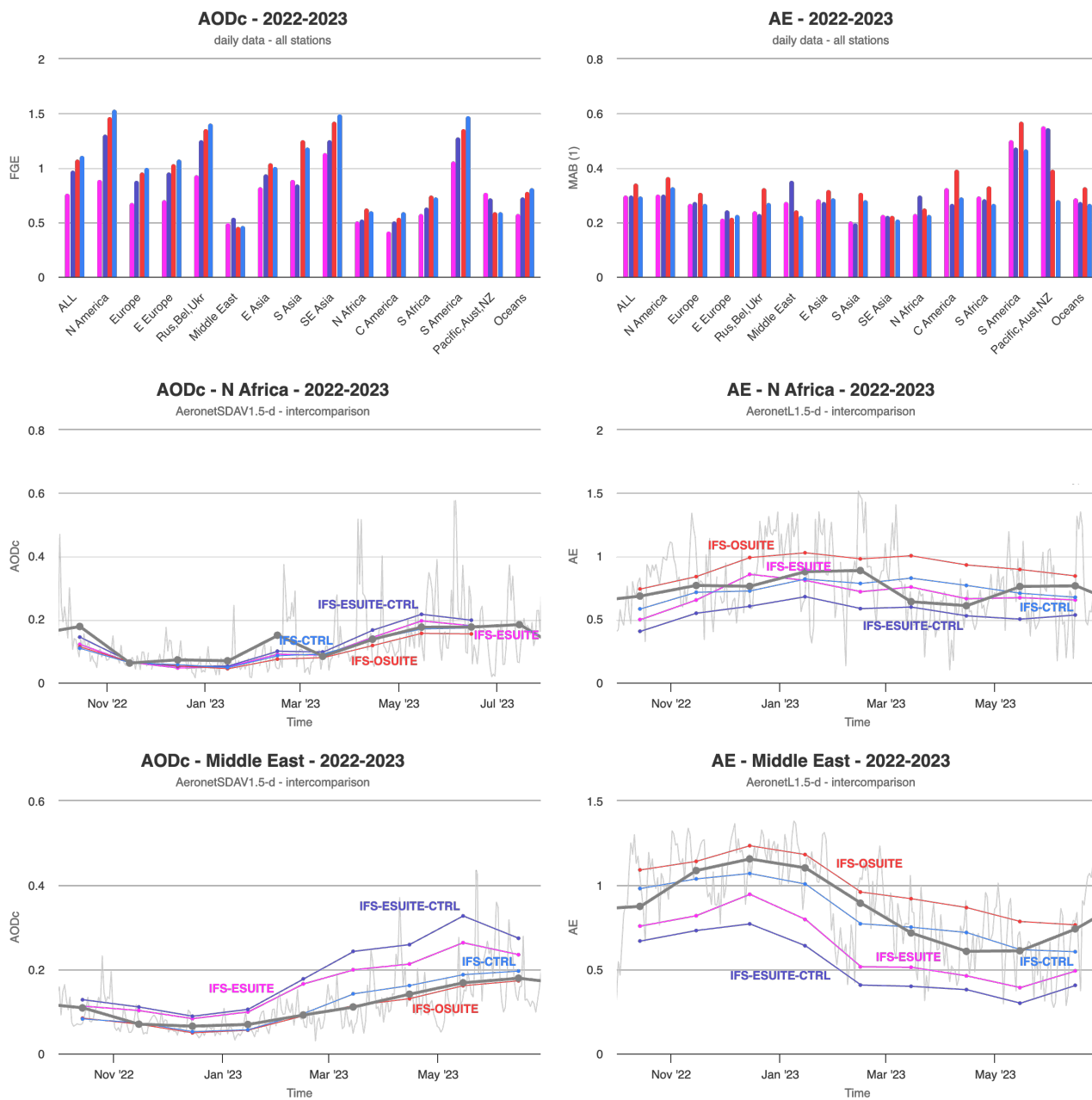
Figure 24. Fractional gross error (FGE) of AOD coarse based on AERONET SDA (Spectral Deconvolution Algorithm) version 3 level 1.5 daily data (left column) and Ångström Exponent between 440nm and 870nm Mean Absolute Bias (MAB) based on AERONET version 3 level 1.5 daily data (right column). The monthly time series (bold lines) along with the daily time series of observations (thin lines) for N. Africa (second row) and Middle East (third row) are also depicted.